KfK 4255
April 1987

Multi-dimensional Neutronics Analysis of the "Canister Blanket" for NET

U. Fischer
Institut für Neutronenphysik und Reaktortechnik
Projekt Kernfusion

Kernforschungszentrum Karlsruhe

KERNFORSCHUNGSZENTRUM KARLSRUHE

Institut für Neutronenphysik und Reaktortechnik
Projekt Kernfusion

KfK 4255

Multi-dimensional Neutronics Analysis of the "Canister Blanket" for NET.

U. Fischer

Kernforschungszentrum Karlsruhe GmbH, Karlsruhe

Kernforschungszentrum Karlsruhe GmbH
Postfach 3640, 7500 Karlsruhe 1

ISSN 0303-4003

Abstract

At KfK a design of a helium-cooled ceramic breeder blanket, called "canister blanket", has been developed for the NET fusion test reactor. In this report a detailed neutronic analysis of the "canister blanket", based on one-, two- and three-dimensional Monte-Carlo calculations in the NET-III double null configuration, is presented.

The main object refers to the three-dimensional analysis of a complete sector of the NET-reactor containing the "canister blanket". This concerns the poloidal distribution of the neutron wall load and the neutron fluxes at the first wall, the spatial distribution of the power density, the total power production and global effects on the tritium breeding ratio. It is shown, that, in case of the "canister blanket", a global tritium breeding ratio beyond 1.0 seems to be feasible for NET.

Mehrdimensionale neutronenphysikalische Analyse des "Kanisterblankets" für NET.

Zusammenfassung

Für den NET-Fusionsreaktor wurde im KfK ein heliumgekühltes keramisches Blanket, das "Kanisterblanket", entwickelt. In diesem Bericht wird, basierend auf ein-, zwei- und dreidimensionalen Monte-Carlo Rechnungen in der NET-III Double Null Konfiguration, eine detaillierte neutronenphysikalische Analyse des "Kanisterblankets" präsentiert.

Den Schwerpunkt bildet hierbei die dreidimensionale Analyse eines Sektors des NET-Reaktors, der mit dem "Kanisterblanket" ausgestattet ist. Dies bezieht sich auf die poloidale Verteilung der Neutronenwandbelastung und der Neutronenflußdichte an der ersten Wand, auf die räumliche Verteilung der Leistungsdichte, auf die gesamte Leistungsproduktion sowie auf globale Effekte in der Tritiumbrutrate. Es ergibt sich für das "Kanisterblanket", daß eine global Brutrate jenseits von 1.0 für NET im Bereich des Machbaren liegt.

Contents

1. Introduction

At KfK a design of a helium-cooled ceramic breeder blanket for the NET fusion test reactor is under investigation /1/. This blanket design, called "canister blanket", has been developed /2,3/ from a conceptual design of a "lobular blanket" by General Atomic /4/.
The canister blanket design is based on an arrangement of self-supporting canisters within a closed first wall vessel (fig. 1-2). The canister contain the breeding material - Li_4SiO_4 pebbles -, the neutron multiplier - slabs of beryllium -, and the helium cooling pipes (fig. 3); helium is used as cooling and purge gas. This design promises a high breeding performance only to its technical construction and the use of the beryllium multiplier in an efficient arrangement /5,6,7/. A global tritium breeding ratio (TBR) beyond 1.0 seems to be feasible for NET, although this is not required.
In this report a detailed neutronic analysis of the "canister blanket" is presented. The analysis is based on one-, two- and three-dimensional (1-, 2-, 3d) Monte-Carlo-calculations for the actual design of the blanket adapted to the NET-III double null (DN) configuration.
Reference is made to previous one-dimensional neutronic calculations showing clearly the merits as the restrictions of such calculations concerning global quantities (TBR, neutron multiplication M), and local ones (e. g. radial distribution of the power density).
The main concern, however, will be the 3d-neutronic analysis of the actual blanket design in the NET-III/DN configuration. This concerns global effects on important quantities (TBR, M), the poloidal variation of the neutron wall load and the neutron fluxes at the first wall, poloidal-radial distributions of the power density, the total power production in the blankets, shields, divertors, vacuum plugs etc..

2. The "Canister Blanket": An Overview

The "canister blanket" uses Li_4SiO_4 - pebbles, enriched to 60% in Li^6, as breeding material, and beryllium as neutron multiplier. The breeding performance of the blanket crucially depends on the arrangement of the beryllium/ceramics configuration. Optimal solutions can be achieved by either mixing beryllium and the breeding ceramics at high volume fractions of beryllium or by using a sandwich-type arrangement /7/. Previous solutions of the "canister blanket" realized these arrangements /1,2,3/. In the actual solution there is only one single beryllium/ceramic zone representing a "homogeneous" beryllium/ceramics mixture, although the arrangement is rather heterogeneous: the Li_4SiO_4 - pebbles are filled in channels between radially-poloidally arranged slabs of beryllium. In contrast to the previous solution /1/, here the pebbles are no longer free to move throughout the canister. This has been achieved by attaching thin sheets of steël at the front, the rear, the top and the bottom of the beryllium slabs /8/. As a consequence of this concept the beryllium/ceramics zone had to be enlarged in order to keep the breeding ratio at an acceptable level, and secondly to reduce the neutron leakage. In the previous solution the beryllium/ceramics zone was followed by a pure Li_4SiO_4 particle bed being roughly 50% thicker than the preceding zone. That solution had a very attractive feature: a relatively high breeding performance at a relatively low beryllium inventory (cf. section 3.1). The actual solution nearly needs twice as much of beryllium inventory in order to keep the breeding ratio at the same level. However, the technical feasibility has been improved considerably by enclosing the ceramic pebbles between the beryllium slabs.

3. One- and Two-dimensional Analyses

3.1 Comparison of ONETRAN and MCNP Calculations

One-dimensional calculations are performed in radial directions in the mid-plane of the torus. The geometrical model used in these calculations is adapted to the NET-geometry by treating inboard and outboard blankets as cylindrical rings around the torus axis. This kind of calculations is very useful in assessing and optimizing the breeding performance of such a blanket.

Furthermore the radial power distribution in the mid-plane is reproduced quite well as compared to realistic three-dimensional calculations (cf. section 4.6). Usually these calculations are performed using the ONETRAN transport programme /9/. In order to have a common base for further comparisons concerning the multi-dimensional Monte-Carlo-calculations, these calculations are performed also using the Monte-Carlo code MCNP /10/ in the same geometrical model. The nuclear data used by ONETRAN are those condensed from the VITAMIN-C-library into a 25 neutron/21 gamma group structure /11/ using the P_3-approximation for the transfer matrices. MCNP uses its own data library in which the nuclear data are represented continously in energy. Essentially these data are based on ENDF/B-IV including important exceptions however. For beryllium e. g. the more recent Los-Alomos evaluation /12/ is used, which is superior to the evaluations contained in ENDF/B-IV and -V (cf. e. g. /13/).

Table I compares the neutron multiplication and the tritium breeding ratio as calculated by ONETRAN and MCNP in the same one-dimensional geometrical model (see sketch in fig.5). It is seen, that the neutron multiplication M and the tritium breeding ratio TBR calculated by ONETRAN, are slightly higher as compared to MCNP; the differences amounting to 0.04 and 0.02, respectively.

This effect essentially is due to the different data for the Be (n, 2n) emission cross-section, where the data contained in the MCNP library are more reliable. Thus in a blanket with Be-multiplier the ONETRAN-calculations usually give an overestimation of the neutron multiplication. Concerning the breeding ratio however, the overestimation in most blankets is lower than 2 %. In contrast to this, the nuclear data describing the energy release (n-and γ -kerma-factors, γ-production cross-sections, etc.), contained in the VITAMIN-C library are more recent and more reliable than those contained in the MCNP-library. The power density calculated by MCNP is systematically lower than that calculated by ONETRAN (table II). The differences on the average amount to ca. 10 %. Based on a fusion power of 600 MW, the ONETRAN calculation gives a total power production (without α-power) of 711 MW for NET, and the one-dimensional MCNP calculation gives 658 MW (see table III). Of course these values are somewhat artifical, because they are based on idealized 1d-calculations; but is seen in section 4.5 that these values are very close to the realistic values for the total power production gained by 3d-Monte-Carlo-calculations. But the key issue from these comparisons is the fact, that the MCNP-calculations - and this holds also for the 3d-calculations presented in section 4 - rather underestimate the nuclear power production.

3.2 Comparison of the Actual and the Previous Design of the "Canister Blanket": 2d-Calculations.

The two-dimensional calculations are performed in radial-toroidal direction in the mid-plane of the torus. In the NET-III/DN configuration, the complete blanket covering the whole surface of the torus will be made of 48 toroidal sectors. Thus a neutronics calculation can be made for one sector, i. e. a 7.5^{o}-segment, representing the total set

of 48 sectors in the case, that all sectors are occupied by the same breeding blanket configuration. Concerning the tritium breeding ratio, it is possible to interpolate linearly between the number of occupied sectors, or, what is equivalent, in the blanket coverage of the torus surface; this is shown explicitely in section 3.3.

An essential feature of a sector of the canister blanket is the fact, that there is no curvature in toroidal direction. This feature facilitates the geometrical modelling of the blanket sector enormously, especially in the three-dimensional calculation (section 4). A further simplification can be achieved by treating only one half of a sector, since the sectors are symmetric as referred to their poloidal mid-plane. Fig. 6 shows a two-dimensional cross-section of a $7.5/2^{\circ}$ segment as it is used in the 2d-calculations.

Based on such 2d-calculations, the tritium breeding ratio of both, the actual and the previous design of the "canister-blanket" are close together, although, based on 1d-calculations, the breeding ratio of the actual design is considerable higher than that of the previous one (table IV). Thus, the impact of the lateral walls (vessel, canister and copper plate, used for passive plasma stabilization) on the neutronic performance of the blanket is stronger in the actual version of the "cansiter blanket" than it is in the previous one. This is a consequence of the enlarged thickness of the beryllium/ceramics-zone and the omission of a pure ceramics-zone. This latter provision is mainly responsible for an enhanced parasitic absorption in the side walls, whereas the former one is the cause for a stronger reduction of the neutron multiplication mainly due to inelastic scattering processes at the structural components of the side walls.

The 2d-calculations, presented here, have been performed with the help of the Monte-Carlo code MCNP /10/ because of it's ease and flexibility in modelling the geometry; furthermore it also has been used for the 3d-calculations presented

in section 4. 2d-calculations of the kind described are a step towards full 3d-calculations (section 4). The main subject of these calculations is the analysis of the lateral walls and their impact on the neutronic performance of the blanket. A further subject of 2d-calculations is the analysis of heterogeneity effects. This has been done already for the previous version of the "canister blanket" and it is just referred here, that the heterogeneous arrangement of beryllium slabs, helium cooling pipes and breeding ceramics can be treated as a homogeneous mixture without any impact on the neutronic performance of the blanket /7/. This means a further simplification for the 2d- and 3d-calculations.

3.3 Dependence of the Tritium Breeding Ratio on the Blanket Coverage.

The 3d-calculations presented in section 4 are performed for one single 7.5^{o}-sector representing all 48 sectors of NET, i. e. it is assumed, that all 48 sectors are occupied by the same breeding blanket configuration. It is however very significant to know the TBR if only some of the sectors are occupied by breeding blankets, but all other by shielding blankets (indeed the strategy for the NET-operation foresees to start with only a small number of occupied sectors and then to increase it step by step /14/): this is the question of the dependence of the TBR on the blanket coverage.

Two-dimensional Monte-Carlo calculations in the mid-plane of the torus are suitable to answer this question. Such calculations have been performed for the previous version of the "canister blanket" in the NET-geometry. Fig. 7 shows the radial-toroidal cross section of the torus in the mid-plane as it is used in these calculations. At the inboard side a simple steel reflector is used. The calculations have been performed for a helium- and a watercooled steel option. All non-breeding sectors have been replaced by shielding blankets containing the same material composition -

i. e. steel, helium - or watercooled - as the inboard steel reflector. Fig. 8 shows the dependence of the TBR on the number of sectors occupied by the canister breeding blanket configuration for both, the helium - as the water-cooled steel option. It can be deduced, that it is valid to interpolate the TBR linearly in the number of occupied sectors, or, what is equivalent, in the blanket coverage. This result may be expressed in a simple formula:

$$TBR\ (Cov) = TBR\ (100) \times Cov$$

where the coverage is defined as:

$$Cov = \frac{\text{number of sectors occupied by breeding blankets}}{\text{total number of sectors}}$$

and TBR (100) is the tritium breeding ratio at full coverage.
As a consequence, the 3d-calculations of a single sector (section 4), representing the complete set of sectors, can also be interpolated linearly in the number of occupied sectors. In other words, the restriction of the 3d-calculation to one single sector is not a restriction for the 3d-calculation itself.

4. Three-dimensional Analysis of the "Canister Blanket"

4.1 Geometrical Model

The 3d-calculationes are also performed with the Monte-Carlo code MCNP /10/. Thus it is possible to use a true geometrical model of the blanket sector without any idealizing approximation. In the present configuration this is achieved only by using planes and cylinders in 3d-space, due to the fact, that within a 7.5^{o}-sector there is no curvature in toroidal direction. Fig. 9 shows a radial-poloidal cross-section of the sector as it is used in these calculations.

Fig. 6 shows a radial-toroidal cross-section of the sector in the mid-plane of the torus.

4.2 Plasma Representation

In the NET-III/DN - configuration, the plasma can be represented by a D-shaped, exponentially decreasing probability distribution for the 14-MeV-source neutrons /15/. The source strength profile is given by /15,16/:

$$s(a) = (1 - (\frac{a}{A})^2)^4 \qquad (1)$$

$$o \leq a \leq A$$

The parametic representation of the plasma contour lines (lines of equal source strength, in Monte-Carlo-terms: lines of equal probability for the emission of a source neutron) is as follows /16,17/:

$$R = R_o + a \cdot \cos (t + \delta \cdot \sin t) + e(1-(\frac{a}{A})^2) \qquad (2)$$

$$z = E \cdot a \cdot \sin t$$

$$0 \leq t \leq 2\pi$$

$$0 \leq a \leq A$$

For the NET-III/DN configuration we have /15/:

R_o	= 518 cm	(plasma major radius)
A	= 135 cm	(plasma minor radius)
E	= 2.18	(elongation)
e	= 16.2 cm	(excentricity)
δ	= 0.65	(triangularity)

R is the radial distance from the torus axis and z is the poloidal distance from the torus mid-plane. Fig. 10 shows the plasma contour map gained with this representation; fig. 11 shows the exponentially decreasing source density profile, equ. (1).

It is this non-uniform spatial plasma distribution correlated with the geometrical arrangement of the blanket sectors around the plasma, which is responsible for the poloidal variation of the neutron wall load, the neutron fluxes and hence the power peaking in the mid-plane of the torus. This will be investigated in detail in section 4.4. In the MCNP-calculation the plasma source distribution is normalized to one source neutron in one half of a sector. In order to normalize to a fusion power of 600 MW (NET-III/DN) a flux normalizing factor of

$$f_\phi = \frac{600\ \text{MeV}}{1.602 \cdot 10^{-19}\,\text{s} \cdot 17.58\ \text{MeV} \cdot 2 \cdot 48}$$

$$= 2.219 \cdot 10^{18}\,\text{s}^{-1}$$

has to be applied.

4.3 Global Tritium Breeding Ratio

For the actual design of the canister blanket a global breeding ratio of TBR = 0.95 is obtained (see table V). This means, that the reduction in the breeding ratio - due to the reduced coverage of the torus in poloidal direction, i. e. essentially these are the divertor openings - is slightly less than the reduction in the coverage: 17 % vs. 20 %. This somewhat incidental agreement is mainly the consequence of the fact, that the source neutrons suffer multiple scattering processes (see section 4.4): On one hand, this effect tends to enlarge the neutron leakage through the openings (more than the direct leakage, corresponding to the coverage of the openings), on the other hand it is resonsible for a considerable neutron current through the top and the bottom of the outboard vessel into the blanket itself. In the configuration analyzed here, these two opposite effects just compensate each other.

Concerning the neutron multiplication, there is no reduction going from the 2d- to the 3d- description: the reduced multi-

plication of beryllium is more than compensated by the enhanced multiplication of the steel components (iron, molybdenum) in the divertors and other non-breeding structural components. This of course leads primarily to parasitic absorptions in the structural components.

The breeding ratio is weakly dependent on the plasma distribution: if a uniform source strength distribution is used (i. e. neglecting the plasma profile, equ. (2)), the TBR drops to 0.91; if furthermore the plasma is shifted to the inboard side of the vacuum chamber, the TBR drops further to ca. 0.85. This behaviour is in agreement with the expected behaviour, since all these provisions reduce the angle, under which the outboard blanket is seen by the source neutrons; hence the 14-MeV-neutron current on the first wall is reduced accordingly - whereas the inboard blanket nearly is not affected.

Replacing the inboard breeding blanket by a single steel reflector - this is an attractive option for NET - would result in a global TBR of 0.80 (table VI). Even if beryllium is used as neutron reflector at the inboard side, this would not improve the TBR, though the neutron multiplication would raise to M = 1.71 in this case (table VI). This behaviour is due to the fact, that the neutrons, gained additionally in (n, 2n) - reactions on beryllium at the inboard side, are well moderated; they are therefore primarily absorbed in the structural material at the inboard side as well as in the first wall of the outboard blanket, before reaching the breeding ceramics in the outboard blanket at all. Thus, for the canister blanket, a beryllium reflector at the inboard side would provide no benefit compared to a simple steel reflector. On the other hand, an alternative option for the inboard blanket would be, to omitt a neutron multiplier at all, but to fill only the breeding ceramics into the canisters at the inboard side. A global breeding ratio of TBR = 0.90 could be achieved in this case (table VI).

It is interesting to investigate, if it would be possible, to achieve a global TBR beyond 1.0 for the canister blanket design within the NET-III/DN-configuration. Without any changes in the design it is possible to increase the TBR by increasing the Li^6 - enrichment to 90%, and further to increase the beryllium/ceramics-zone at the outboard side by 6 cm (this space is still available within the canister). Thus a global TBR of 0.98 and 1.02, respectively, would be obtained (table VII).

Based on experiences gained by one dimensional analyses /6/, it is expected, that the insertion of a hydrogeneous moderator (e. g. $ZrH_{1.7}$) in the outer blanket regions would also raise the global TBR beyond 1.0, although this has not been proven by 3d-calculations (of course this would necessitate a serious change in the technical construction of the blanket).

A global TBR of 1.02 is also obtained, if the graphite protection layer of the first wall is omitted (table VIII). The gain in the breeding ratio by this hypothetic provision is however very moderate as compared to the 1d-calculations, namely being 0.07 and 0.15, respectively. This shows, that the usual 1d-calculation overestimates the significance of the first wall on the neutronic performance of the blanket, because the neutron do not enter the blanket only through the first wall, but also - and this refers especially to the outboard blanket in the NET-III/DN-configuration - through the top, the bottom and the lateral walls of the vessel and the canister.

4.4 Poloidal Variation of the Neutron Wall Load and the Neutron Fluxes at the First Wall

Poloidal variations of the neutron wall load, the neutron fluxes, reaction rates, energy release rates etc., are primarily caused by a non-uniform plasma distribution correlated to the geometrical arrangement of the blanket sectors, which in general are not well adjusted to the spatial plasma distribution. In the NET-III/DN-configuration e. g. we have a plane inboard blanket; only the outboard blanket is approximated in it's poloidal curvature to the plasma contour lines (fig. 9). Furthermore, there is a strong decrease of the source density in going outwards from the plasma centre (fig. 11). Therefore the neutron source is concentrated in the region near the mid-plane and close to the plasma major radius (the maximal source density is at $R = R_0 + e = 534$ cm in the mid-plane, see equ. (1)). As a consequence, the neutron wall load - defined as the 14 MeV-neutron current impinging on the first wall - is peaked at the mid-plane of the torus and decreases rapidly as the poloidal distance to the mid-plane is increasing (fig. 12). Clearly, the peaking of the wall load is pronounced the more, the stronger the curvature of the first wall deviates from the curvature of the plasma contour lines. Thus we have a peaking factor 2.0 at the inboard, and only 1.38 at the outboard side.

Fig. 13 illustrates the strong sensitivity of the poloidal wall load distribution to the spatial plasma distribution. Some extreme - rather artifical - spatial plasma distributions have been created to analyze this sensitivity.

For a uniform source distribution within the whole vacuum chamber the wall load distribution clearly will be rather flat; only near the top and the bottom of the inboard blanket there will be a slight decrease, because at this level there is the plasma boundary. For the outboard blanket this does not hold, because - due to it's curvature - it encloses the plasma.

If we divide now the vacuum chamber into two halves and restrict the same uniform plasma distribution to the inner half of the chamber, the poloidal wall load distribution of course will not change qualtitatively, in case of the inboard blanket, but, because of it's curvature, this will be observed in case of the outboard blanket: as seen from the inner vacuum chamber, equal poloidal emission angles correspond to smaller areas at the top and the bottom of the outboard first wall than at the mid-plane. Therefore, the same area at the top and the bottom will be hit by more neutrons than in the mid-plane; consequently the wall load at the outboard blanket increases as the poloidal distance increases in this case (fig. 13).

This is the key point in the poloidal variation of the neutron wall load: the relation between equal poloidal emission angles of the source neutrons and the corresponding areas of the first wall, depending on the spatial distribution of the source neutrons and the geometrical arrangement of the covering blankets. Thus it is clear, that a hypothetical point source (situated near the centre of the curvature of the outboard blanket, i. e. near the inboard first wall) will result in a very flat wall load distribution for the outboard blanket, but in an extreme poloidal variation for the inboard blanket. For a hypothetical line source (in poloidal direction) on the other hand, the poloidal distribution for the inboard blanket will be rather flat, but now it will vary extremely in case of the outboard blanket showing a deep minimum at the mid-plane.

Returning to the reälistic plasma distribution in the NET-III/DN-configuration, it is interesting to compare the average neutron wall load for the inboard and outboard blanket gained by the 3d- and the 1d-calculations. In case of the 3d-calculations, we have 0.72 MW/m^2 at the inboard blanket, and 1.27 MW/m^2 at the outboard blanket (table VIII).

In case of the 1d-calculations, these values are 0.77 MW/m^2 and 1.13 MW/m^2, respectively (table IX). The average wall load is of course 1.0 MW/m^2 . In case of the 3d-calculation the average wall load is 1.08 MW/m^2, because the first wall (outboard and inboard blanket) does not cover the whole surface. Clearly, the wall load is also 1.0 MW/m^2 if the divertor openings are accounted for. Thus, due to its geometrical restrictions, 1d-calculations underestimate the neutron wall load at the outboard blanket significantly. It will become clear, however, that this is no serious restriction of the 1d-calculation itself, because it is not the neutron wall load, i. e. the 14-MeV-neutron current on the first wall, but the total neutron flux, which is the genuine physical quantity, that - together with the nuclear cross-sections - determines the raction rates and hence the neutronic performance of the blanket.

The poloidal distribution of the neutron wall load already had been calculated by C. Ponti for a water cooled LiPb-blanket in the NET-II/A-single null - configuration /17/. Fig. 19. compares that distribution with the one calculated here for the "canister blanket" in the NET-III/DN-configuration. It is seen, that in case of the outboard first wall both distributions agree very well, whereas in case of the inboard first wall, the distribution calculated by Ponti is much more flatter. This mainly may be traced back to the difference between the single null and the double null configuration, involving a different plasma distribution, affecting only the inboard side, but - due to it's curvature - not the outboard side.

Recent calculations, performed by K. A. Verschuur for the NET-watercooled LiPb - blanket in the NET-III/DN-configuration /18/, compare very favourable with the calculations for the "canister blanket": there the average neutron wall load is 0.71 and 1.19 MW/m^2, inboard and outboard side, respectively, and the peaking factors are 1.6 and 1.30, respectively.

Thus the poloidal profile at the inboard side is slightly flatter; this may be due to slight differences in the configuration of the blanket and the divertors.

In contrast to the strong poloidal variation of the neutron wall load (fig. 12), the poloidal distribution of the neutron flux at the first wall is rather flat (fig. 14). This is due to the fact,that the 14-MeV-neutrons impinging on the first wall suffer multiple scattering processes,resulting in a total neutron flux, which is on the average one order of magnitude larger than the 14-MeV-neutron current (table IX). The peaking values of the total neutron fluxes are 1.21 and 1.11, inboard and outboard blanket, respectively (table IX). The 1d-calculation gives a neutron flux which is on the average 21 % higher as compared to the 3d-calculation, although the 14-MeV-neutron current is underpredicted by the 1d-calculation. This is of course a consequence of the fact, that the plasma is completely covered by the blankets in the 1d-calculation. But it is this mechanism, that finally is responsible for the reliability of the 1d-calculation performed in the mid-plane: although the neutron wall load is underpredicted considerably (it is truely 1.75 MW/m^2 in the mid-plane at the outboard first wall, cf. fig. 12), the total neutron flux at the first wall is overestimated (by 10% as compared to the true value in the mid-plane at the outboard first wall).
This kind of "artificial lifting" of the neutron flux - due to the geometrical model used - finally assures the reliability of the 1d-calculation: the total power production of the configuration as a whole, and the radial distribution of the power density in the mid-plane are reproduced very satisfactorily as compared to the 3d-calculations. This rather unexpected feature is however not valid in general; it depends to a high extent to the specific configuration.

4.5 Total Power Production

The 3d-Monte-Carlo-calculations give a total power production (without α - power) of 695 MW for the "canister blanket" in the NET-III/DN configuration. This emplies an energy multiplication of 1.45 (table X). These values are in very good agreement with those gained by the 1d-calculations (table X), although the comparison between different 1d-calculations, performed with MCNP and ONETRAN (section 3.1), suggests, that the power production calculated by MCNP should be higher by 10%. It is expected, however, that the true power production will be only a few percent higher than predicted by the 3d-Monte-Carlo-calculation.

In the 1d-calculation, the whole power of course is produced only in the blankets (including the radial shields), the contributions of the inboard and outboard blankets amounting to 27% and 73%, resprectively (table X). In the realistic 3d-calculation, however, only 84% of the total power is produced in the blankets (20% inboard and 65% outboard); about 9% is produced in the divertors and 7% in the remaining components of the sector (plugs, shielding components), see table X.

Comparing 1d- and 3d-calculations, we have good agreement in the total power production, but due to the geometrical model used in the 1d-calculation, there is a "power shifting" into the blankets. This somewhat artificial "power shifting" - which per se results in an overestimation of the power production in the blankets themselves (table X) - on the other hand just simulates the power peaking in the mid-plane -; in case of the "canister blanket" in the NET-III/DN-configuration incidentally at the right level: it is this artificial "power shifting" that is responsible for the good agreement of the radial distribution of the power density in the mid-plane as compared to the 3d-calculation (section 4.6).

Furthermore, it is seen, that the 1d-calculation underestimates the power production in the outboard shield considerably (table X): the 1d-model of course is not able to account for the strong neutron current through the top and the bottom of the outboard vessel into the shield. This may indicate, that shielding problems have to be expected in these regions: this has to be investigated. At the inboard side, this effect is not observed, because there the blanket is shielded by the divertors.

4.6. Radial-Poloidal Distribution of the Power Density

The poloidal distribution of the power density, gained by the 3d-calculation, is reproduced in fig. 15 and 16 for various radial divisions. It is seen, that the poloidal profile of the power density rather reflects the poloidal distribution of the neutron flux than that of the neutron wall load. The peaking factors are typically around 1.40 and 1.20, inboard and outboard blanket, respectively.

In case of the outboard blanket, the poloidal profile of the power density flattens as one propagates into the blanket, reaching finally a nearly uniform distribution at the rear wall of the vessel (fig. 15). This behaviour is due to the geometrical construction of the outboard blanket within the NET-III/DN configuration: there is a considerable neutron current through the top and the bottom of the outboard vessel (see fig. 9), lifting the neutron flux in the rear part of the blanket, the more, the larger the distance is to the mid-plane (cf. fig. 15). Indeed, the power density in the top and the bottom wall of the outboard vessel (fig. 17) radially decreases only to ca. 50 % within the first 25 cm and remains at a constant level the next 40 cm up to the rear of the vessel. In case of the rear walls (canister, vessel) the power density at the top and the bottom is nearly twice as high as it is in the mid-plane.

At the inboard side, the blanket vessel is shielded at the top and the bottom by the divertors; therefore the poloidal profile of the power density does not change, as one propagates into the blanket (fig. 15,16). This becomes even clearer, if the radial profile of the power density is compared at different poloidal levels (fig. 18). It is seen, that the profiles at the inboard side are equal - there is only a shifting of the level -, whereas the profiles at the outboard side change with the poloidal level. There is the strongest radial gradient of the power density at the mid-plane and the weakest one at the top and the bottom. That is, the radial decrease of the power density becomes weaker with increasing poloidal distance to the mid-plane.

As can be seen from fig. 18, the 1d-calculation, performed in the mid-plane of the torus, quite well reproduces the radial distribution of the power density in the mid-plane, as it is obtained by the 3d-calculation. Especially this holds in case of the outboard blanket. That is, concerning the power production, the 1d-calculation is able to simulate the reality as it is given in the mid-plane (including the power peaking there!), although such a kind of calculation contains no information on the poloidal or toroidal direction, and, although the total power production agrees with the true one (in this respect, the 1d-calculation should give a kind of a representative description of the whole blanket). The cause of this rather astonishing feature of the 1d-calculation has been discussed already in the preeding section 4.5: it is the "power shifting" from divertors and poloidal arranged shielding components into the blanket themselves. Incidentally, this artifical "power shifting", which is only due to the idealized geometrical model used in the 1d-calculation, in case of the "canister blanket", just shifts the power production to that level, which in reality is reached in the mid-plane (in a rigorous sense, the "right level" is reached only for the outboard blanket, whereas for the inboard blanket

it is slightly underestimated, see fig. 18). But in reality this power peaking in the mid-plane of course is caused by the geometrical arrangement of the blanket sectors, divertors etc. in correlation with the spatial plasma distribution. Therefore, the reliability of the 1d-calculation, performed in the mid-plane of the torus, cannot be assured a priori for any blanket configuration. If any other configuration is considered - e. g. a single null configuration, a different blanket design or only a different geometrical arrangement of the same blanket - it has to be proven, that the corresponding 1d-calculation is reliable in the same sense. This has been proven here for the "canister blanket" in the NET-III/DN-configuration.

5. Conclusion

A detailed neutronics analysis of the "canister blanket" design in the NET-III/DN-configuration has been performed. A true geometrical model of a complete 7.5^{o} sector - without any idealizing approximations - has been treated by means of multidimensional Monte-Carlo calculations.

It has been shown, that the "canister blanket" has the potential, to reach a global breeding ratio beyond 1.0. For the standard design of the "canister blanket", a global breeding ratio of 0.95 has been obtained. In case the inboard blanket is replaced by a neutron reflector, the global breeding ratio would be 0.80.

It has been observed, that the global breeding ratio can be interpolated linearly in the number of sectors occupied by a breeding module. Furthermore, it has been observed, that global effects on the breeding ratio are sensitive to the special blanket design. It is pointed out, that in case of the actual canister blanket the reduction in the breeding ratio due to the divertor openings is slightly smaller than the reduction of the blanket coverage itself. There is also a weak sensitivity of the global tritium breeding ratio on

the spatial distribution of the plasma.

The poloidal variation of the neutron wall load is extremely sensitive to the plasma distribution. In a realistic representation of the NET-III/DN plasma distribution, there is a strong poloidal variation of the neutron wall load, the peaking factors being 1.38 and 2.0, outboard and inboard first wall, respectively. On the other hand, the poloidal distribution of the more significant total neutron flux is somewhat flatter; the same holds for the poloidal distribution of the power density. Due to the geometrical construction of the outboard blanket the poloidal variation of the power density flattens, as one propagates into the blanket. For the inboard blanket this feature is not observed, because it is shielded by the divertors.

Comparing the usual 1d-calculation - performed in the mid-plane of the torus - and the 3d-calculation, it is interesting to note, that the total power production, amounting to 695 MW in the 3d-calculation, is also obtained in the 1d-calculation. On the other hand, the 1d-calculation also reproduces the radial power distribution of the 3d-calculation in the mid-plane quite well - without applying any poloidal peaking factor. This rather astonishing feature of the 1d-calculation can be explained by a kind of "power shifting" due to the geometrical model used. Incidentally the level of this artifical "power shifting" is just right to reproduce the true power peaking in the mid-plane. In this respect, the 1d-calculation has been proven to be very powerful and reliable. It is pointed out, however, that this feature doesn't need to be valid in general: it is strongly dependent on the blanket design and the configuration of the plasma and the divertors. It has been proven here for the "canister blanket" in the NET-III/DN-configuration.

Acknowledgement

I would like to thank M. Küchle for the critical reading of the manuscript and Mrs. M. Beck for the typing of the manuscript.

References

/1/ M. Dalle Donne, U. Fischer, G. Sordon, E. Bojarski, H. Reiser, P. Norajitra, E. Bogusch: Pebble Bed Canister, a Ceramic Breeder Blanket with Helium Cooling for NET, 14th Symp. Fus. Techn., Avignon, 8.-12. Sept. 1986.

/2/ M. Dalle Donne, U. Fischer, E. Bojarski, H. Reiser: Pebble Bed Canister, a Ceramic Breeder Blanket Design with Radial Helium Cooling, NET-Blanket Engineering Meeting on Solid Breeder Blankets, Karlsruhe 26.-28. Nov. 1985.

/3/ M. Dalle Donne, U. Fischer, E. Bojarski, H. Reiser: Pebble Bed Canister, a Ceramic Breeder Blanket with Helium Cooling for a Fusion Reactor, ENC-4, International ENS/ANS-Conference, Geneva, 1.-6. June, 1986.

/4/ M. A. Abdou et al.: Blanket Comparison and Selection Study, Report ANL/FPP-83-1, 1983.

/5/ U. Fischer: Neutronics for the Pebble Bed Canister Blanket, NET-Blanket Engineering Meeting on Solid Breeder Blankets, Karlsruhe, 26.-28. November 1985.

/6/ U. Fischer: KfK 1986, Unpublished report.

/7/ U. Fischer: Optimal Use of Beryllium for Fusion Reactor Blankets, 14th Symp. Fus. Techn. Avignon, 8.-12. Sept. 1986.

/8/ E. Bojarski, H. Reiser: personal communication, December 1986.

/9/ T. R. Hill: ONETRAN, a Discrete Ordinates Finite Element Code for the Solution of the One-dimensional Multigroup Transport Equation, LA-5990-MS (1973).

/10/ Los Alamos Monte Carlo Group: MCNP - A General Monte-Carlo Code for Neutron and Photon Transport, Version 2B, Los Alamos 1981.

/11/ R. T. Perry, G. A. Moses: A Combined P_3, VITAMIN-C, MACK-IV, coupled 25 Neutron-21 Gamma Group Cross Section Library, UWFDM-390, University of Wisconsin (1980).

/12/ P. G. Young, L. Stewart: Evaluated Data for n + ^{9}Be-Reactions, LA-7932-MS (1979).

/13/ M. Z. Youssef, M. A. Abdou: Uncertainties in Production of Tritium Breeding in Candidate Blanket Designs due to present Uncertainties in Nuclear Data Base, Fus. Techn. 9 (1986), 286-307.

/14/ M. Chazalon, P. Libin: Strategy of Breeding Blanket Introduction in NET and Testing Requirements, 14th Symp. Fus. Techn., Avignon, 8.-12. Sept. 1986.

/15/ W. Dänner, NET-Team, personal communication, December 1986.

/16/ K. A. Verschuur: FURNACE, A Toroidal Geometry Neutronic Program System - Method Description and User Manual, Report ECN-162 (1984).

/17/ C. Ponti: Poloidal Distribution of Neutronic Responses on the First Wall, Ad hoc Working Party on NET Blanket Design, Ispra, 27.-28. Nov. 1984.

/18/ W. Dänner, M. Rieger, K. A. Verschuur et al.: Progress in Design and Analysis of the NET Water Cooled Liquid Breeder Blanket, 14th Symp. Fus. Techn., Avignon, 8.-12. Sept. 1986.

	MCNP	ONETRAN
M	1.72	1.76
TBR	1.27	1.29

Table I: 1d breeding ratio for the actual canister blanket

		MCNP	ONETRAN
canister rear wall	inboard	3.34	3.48
Be/ceramics		5.19	4.98
canister first wall		6.96	7.27
vessel first wall		7.75	8.07
graphite		4.55	5.95
graphite	outboard	6.50	9.39
vessel first wall		10.74	11.98
canister first wall		9.58	10.72
Be/ceramics		3.39	3.63
canister rear wall		0.765	0.948

Table II: Comparison of the power density (W/cm^3) as calculated by ONETRAN and MCNP (1d-calculations).

	MCNP	ONETRAN
Energy release (MeV/fusion)	19.29	20.8
Energy multiplication	1.37	1.48
Total power * (MW) (only neutrons)	658	711
Total power * (MW) (incl. α-power)	778	831

Table III: Comparison of the total power production as calculated by ONETRAN and MCNP (1d-calculations).

* based on a fusion power of 600 MW

		previous design /1/	actual design
M	1d	1.57	1.72
	2d	1.53	1.63
TBR	1d	1.17	1.27
	2d	1.12	1.15

Table IV: Tritium breeding ratio and neutron multiplication for the previous and the actual design of the "canister blanket", based on 1d- and 2d-MCNP-calculations.

	3d	2d	1d
M	1.66	1.63	1.72
TBR	0.95	1.15	1.27
inb.	0.17	0.26	0.29
outb.	0.78	0.89	0.98

Table V: Tritium breeding ratio for the actual canister blanket design gained by 1d-, 2d- and 3d- Monte-Carlo-calculations.

inboard:	steel	beryllium	ceramics (only)
M	1.59	1.71	1.58
TBR	0.80	0.81	0.90

Table VI: Global tritium breeding ratio for different options for the inboard side of the canister blanket.

option	no graphite tiles	90 % Li^6-enrichment	
			enlarged Be/ceramics-zone outboard
M	1.76	1.66	1.67
TBR	1.02	0.98	1.02

Table VII: Global tritium breeding ratio for alternative options of the canister blanket.

	J_{14} ($10^{13}cm^{-2}s^{-1}$)	Wall Load (MW/m^2)	ϕ_{tot} ($10^{14}cm^{-2}s^{-1}$)	ϕ_{fast} ($10^{14}cm^{-2}s^{-1}$)
inboard	3.21	0.72	3.85	2.17
outboard	5.62	1.27	4.42	2.62
average	4.77	1.08	4.22	2.46
	J_{14}	Wall Load	ϕ_{tot}	ϕ_{fast}
ratio outb./inb.	1.75	1.75	1.15	1.21
peaking value				
inboard	2.0	2.0	1.21	1.36
outboard	1.38	1.38	1.11	1.17

Table VIII: Average values for the 14-MeV neutron current (J_{14}), the total and the fast (E > 0.1 MeV) neutron flux at the first wall of the inboard and outboard blanket (based on 3d-calculations).

	J_{14} ($10^{13}cm^{-2}s^{-1}$)	Wall Load (MW/m^2)	ϕ_{tot} ($10^{14}cm^{-2}s^{-1}$)
inboard	3.41	0.77	4.64
outboard	5.01	1.13	5.38
average	4.44	1.00	5.11
	J_{14}	Wall Load	ϕ_{tot}
ratio outb./inb.	1.47	1.47	1.16

Table IX: Wall load, 14-MeV-neutron current and total flux at the first wall (based on 1d-calculations).

	3d (MCNP)		1d
	7.5°-sector	whole blanket	ONETRAN
inboard	2.85	136.7	194.8
blanket	2.19	105.0	161.1
shield	0.66	31.7	33.7
outboard	9.36	449.2	515.9
blanket	8.21	394	497.8
shield	1.15	55.2	18.1
divertors	1.28	61.6	--
remaining components	0.98	47	--
total power(neutr.)	14.47	694.5	710.7
energy multi-plication	1.45	1.45	1.48
total power (ind. α-power)	16.97	814.5	830.7

Table X: Balance of the power production (MW) of the "canister blanket" in the NET-III/DN-configuration (based on 1d- and 3d-calculations).

8. Figures

General remarks concerning the graphical representation of the results from the Monte-Carlo-calculations:

The accuracy of Monte-Carlo-calculations crucially depends on the number of events for a given quantity. In case of global quantities, like the tritium breeding ratio or the neutron multiplication, it is sufficient to follow the tracks of 10.000 to 20.000 source neutrons in order to obtain a statistical error around 1 %. In case of local quantities, like the distribution of the power density, up to 100.000 source neutrons are needed to assure on the average a statistical error around 5%. In all figures, except one (fig. 19), the results of the Monte-Carlo-calculations are presented as histograms, i. e. only the "true values" of the calculation itself are given - in the same bins that are used by the calculation. Thus, a good feeling of the statistical uncertainties is obtained just by regarding the histogram as a whole. Therefore, it does not seem to be necessary to include error bars, as it would be the case if - instead of the "true values" - interpolated values in a smoothly fitted curve (cf. e. g. fig. 19) would be used.

INTERATOM

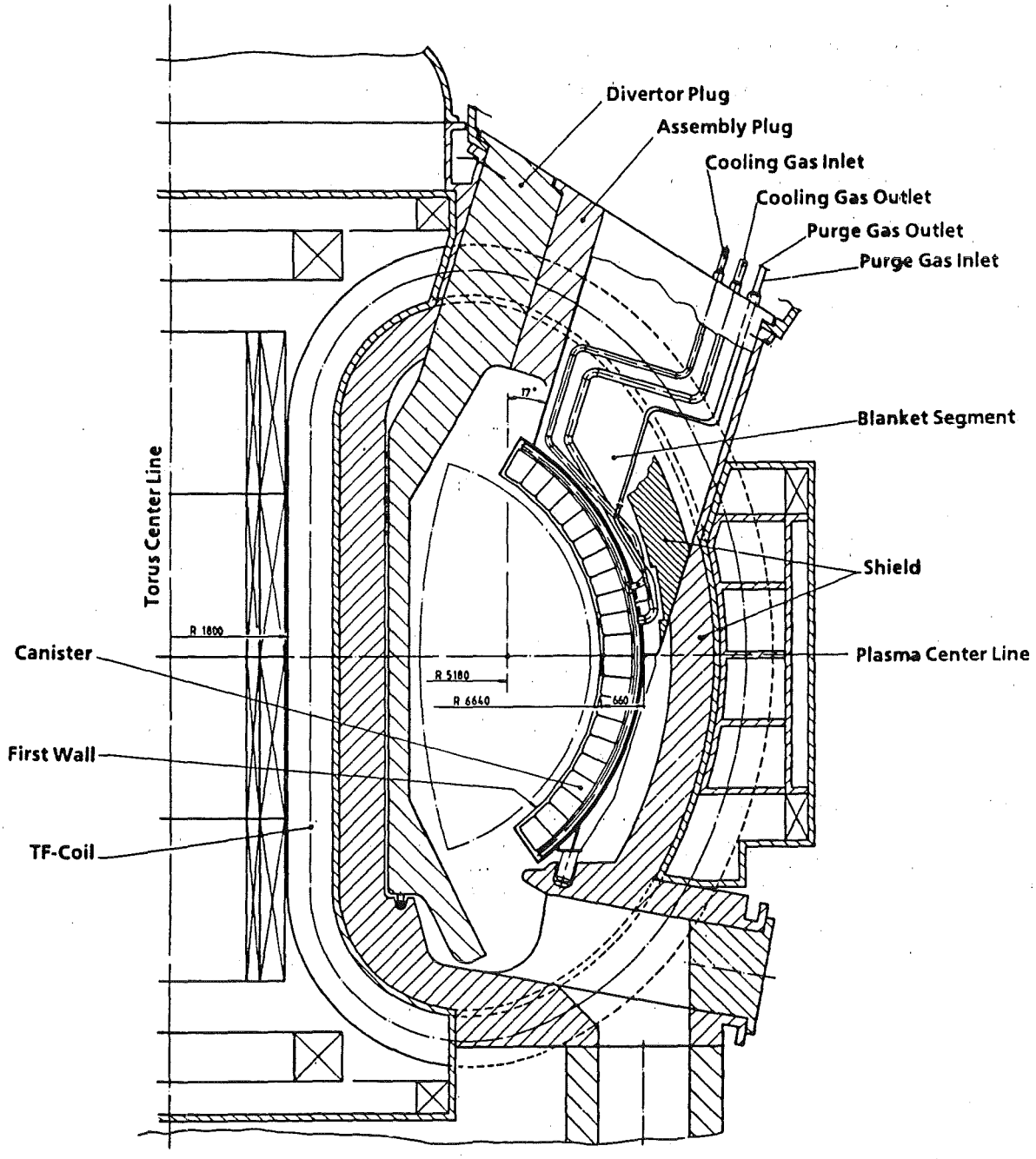

FIG. 1: POLOIDAL CROSS SECTION OF THE NET-III/DN CONFIGURATION INCLUDING THE "CANISTER BLANKET".

(dimensions in mm)

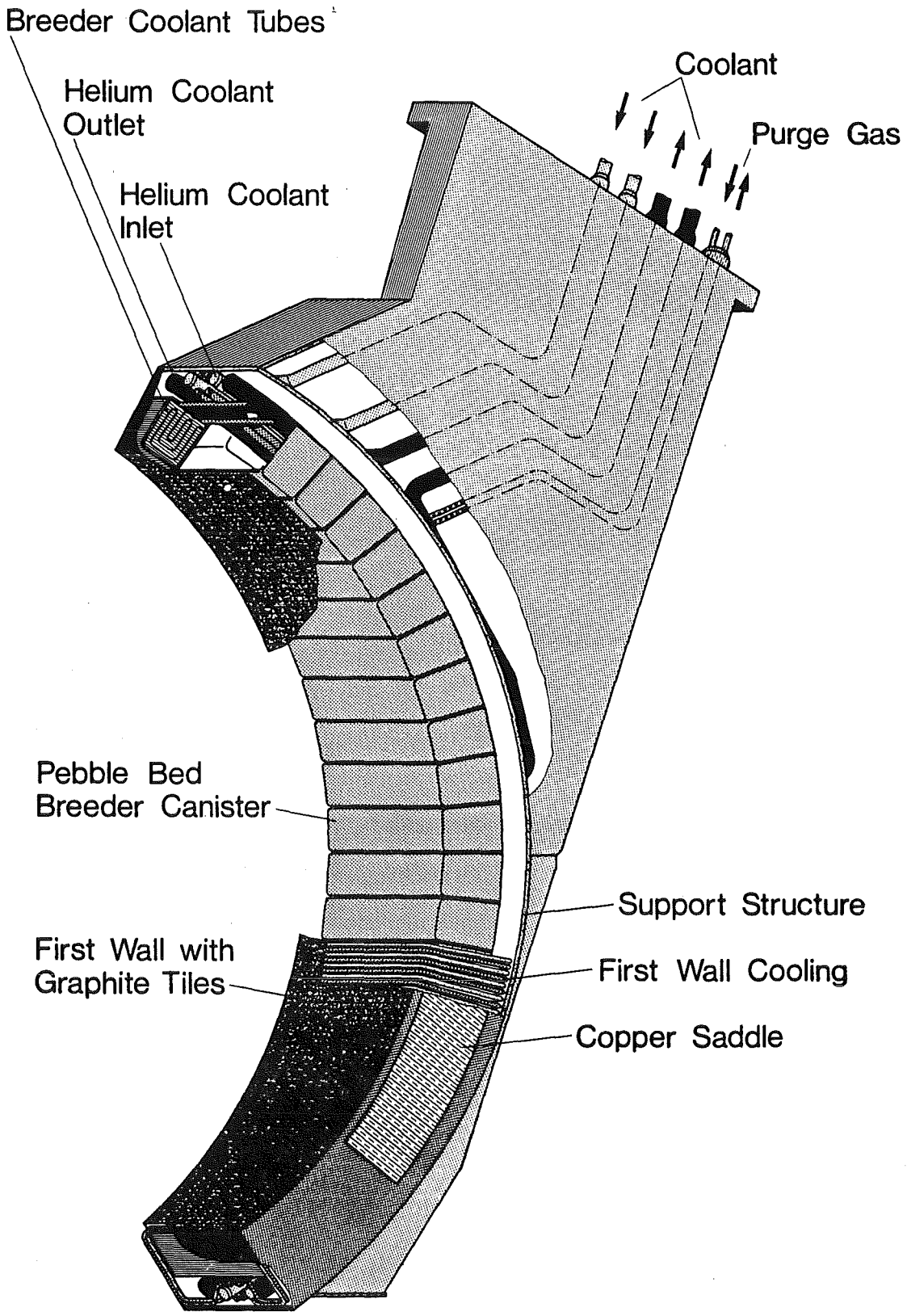

FIG. 2: OUTBOARD SEGMENT OF THE "CANISTER BLANKET".

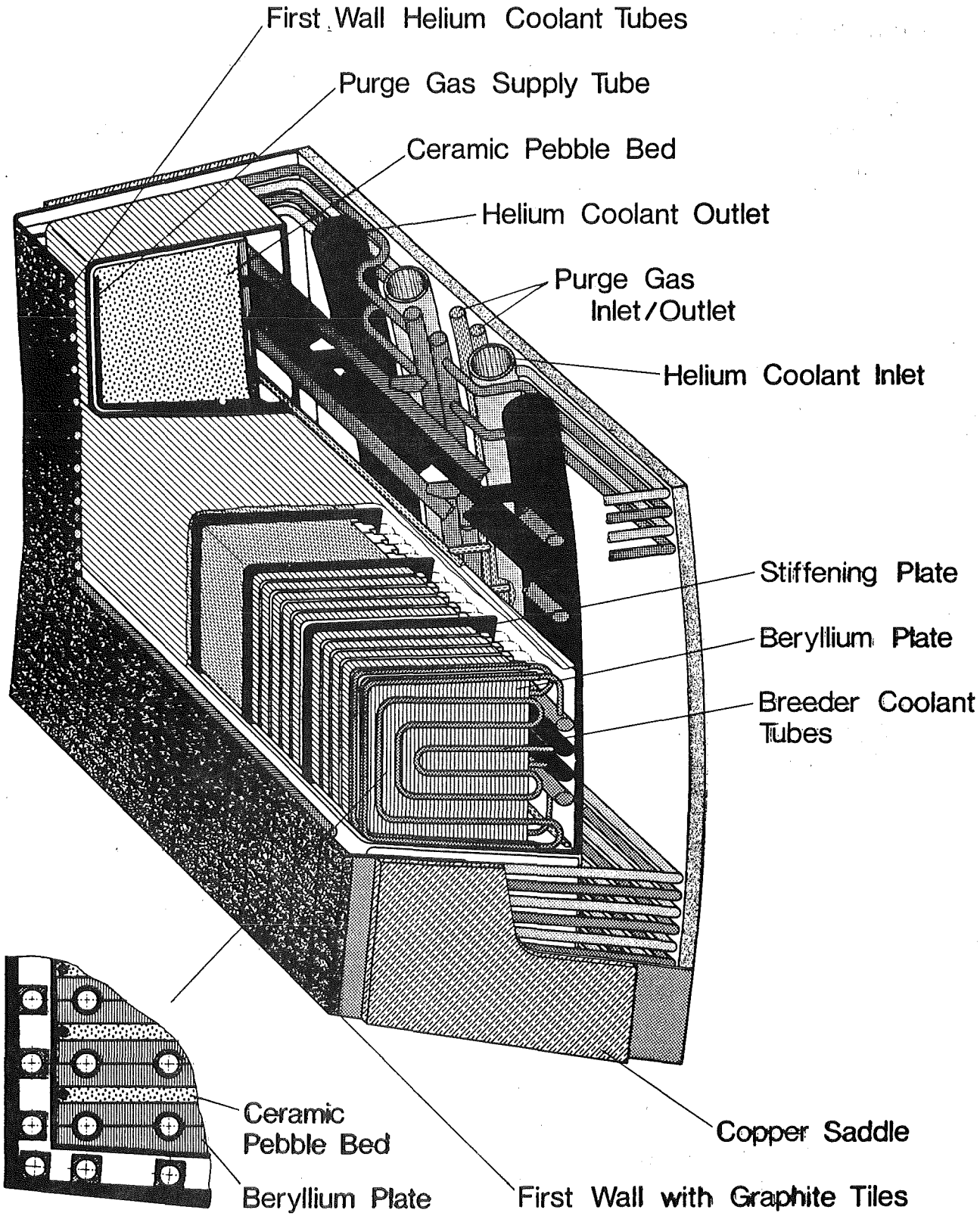

FIG. 3: VIEW OF A CANISTER

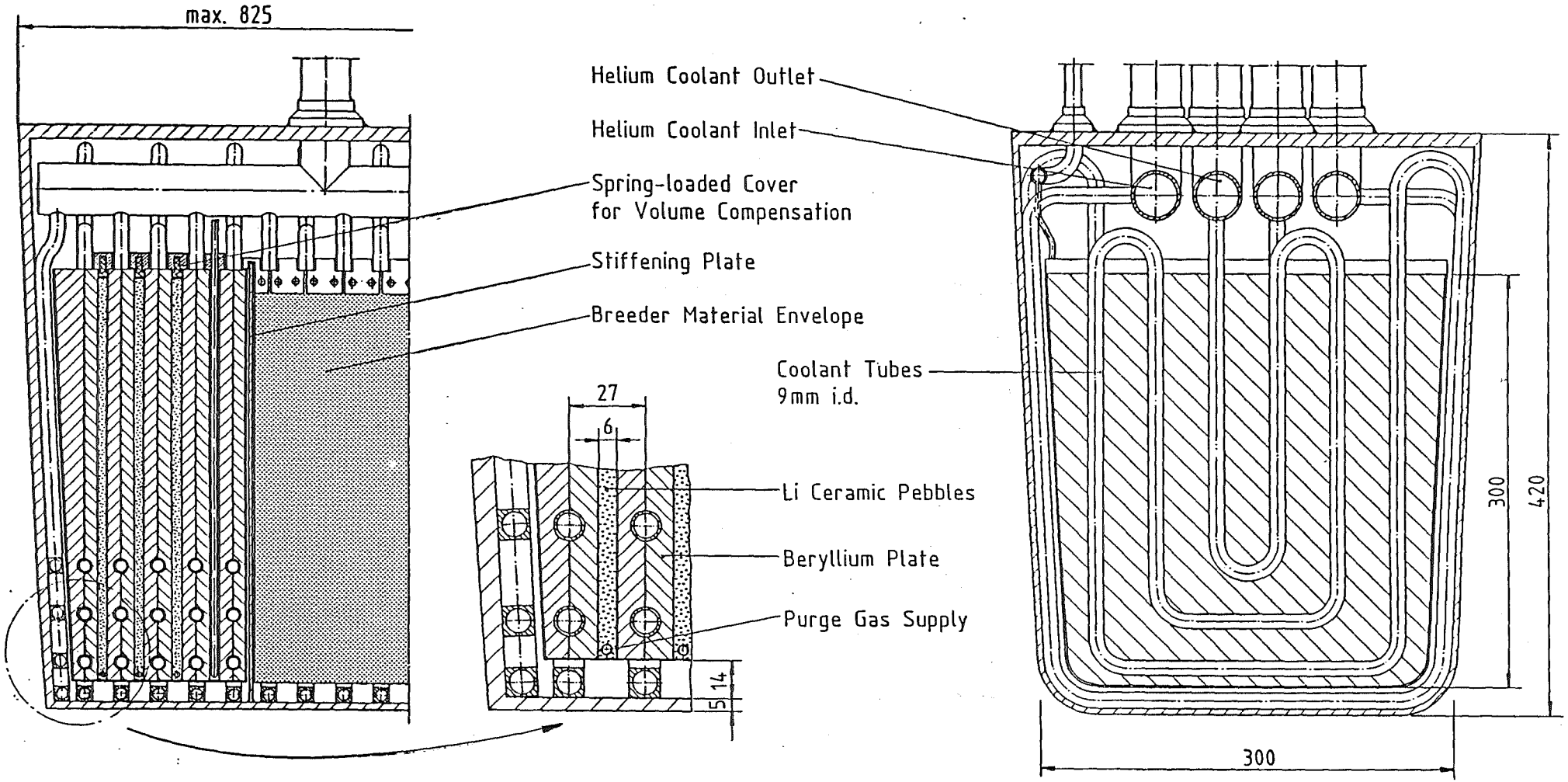

FIG. 4: RADIAL-TOROIDAL AND RADIAL-POLOIDAL CROSS-SECTION OF A CANISTER.

Kernforschungszentrum Karlsruhe, IMF III, Jan. 87

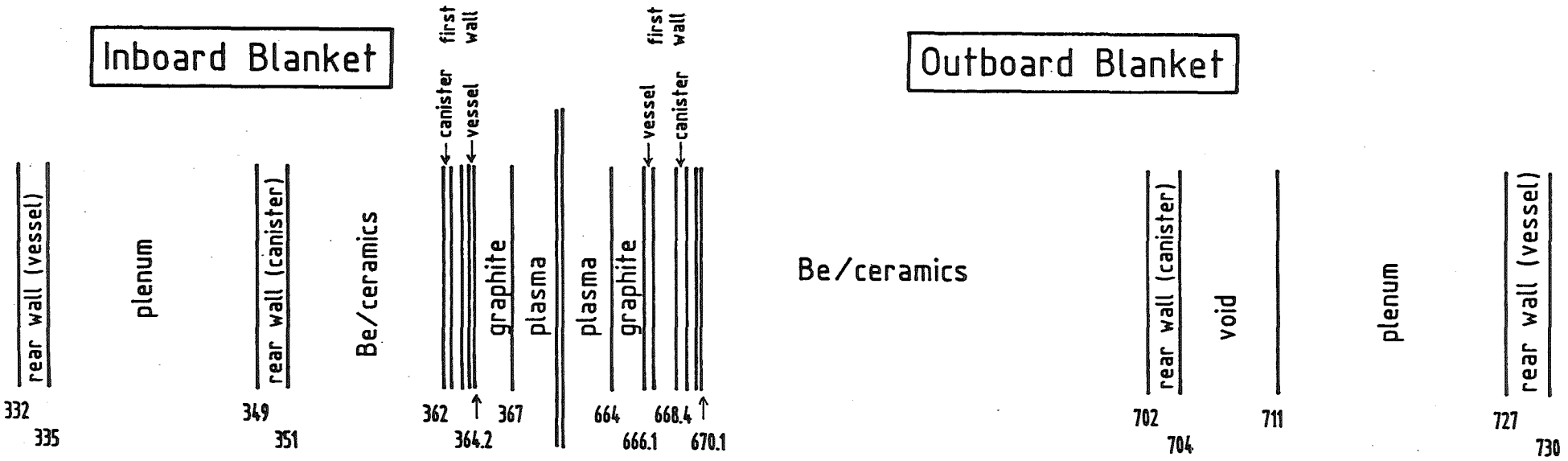

Fig. 5: Sketch of the one-dimensional geometrical model in the mid-plane of the torus (actual "canister blanket" design)

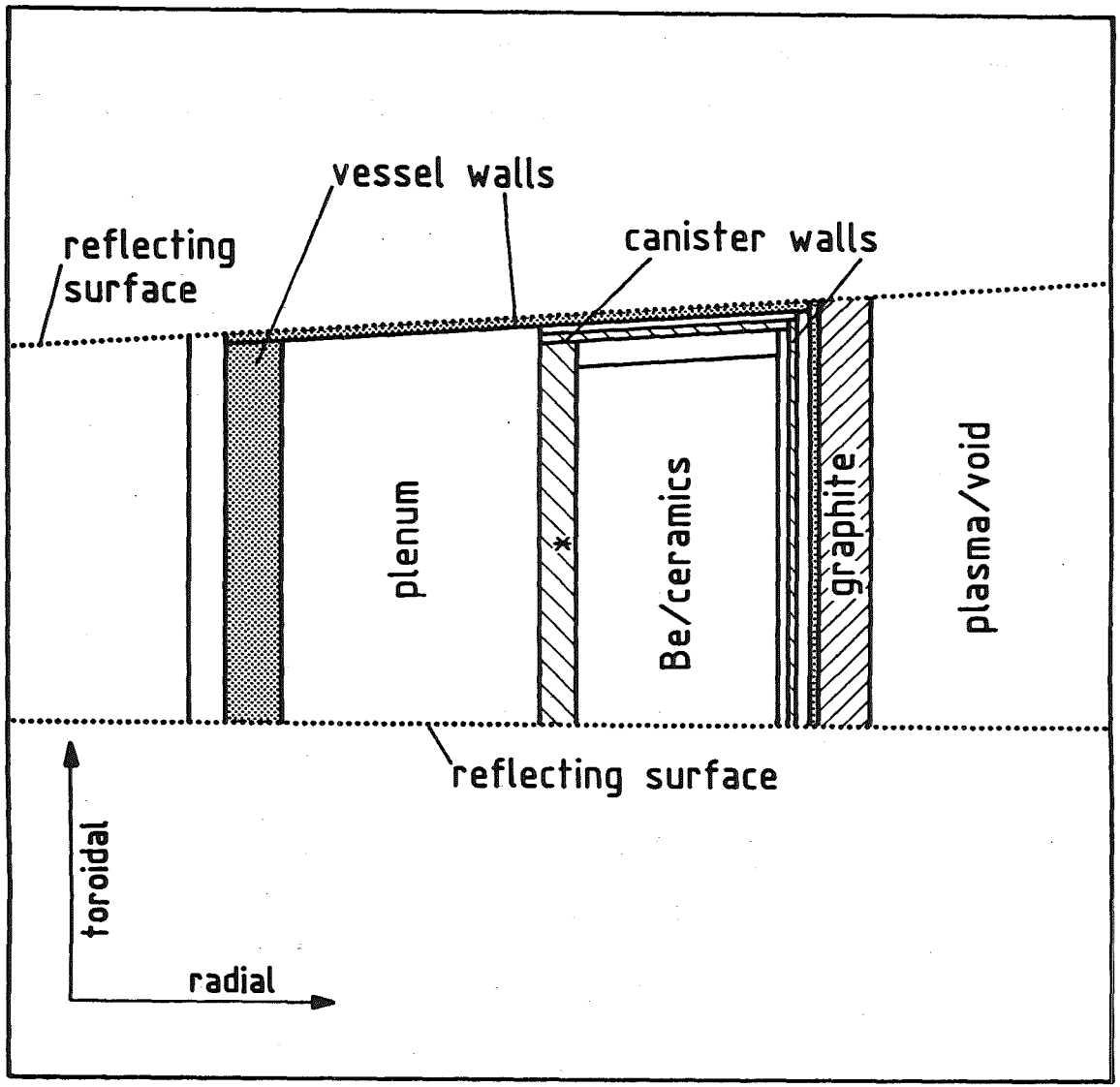

Fig. 6a: Radial-toroidal cross-section of the inboard blanket (half of a 7.5°-sector)

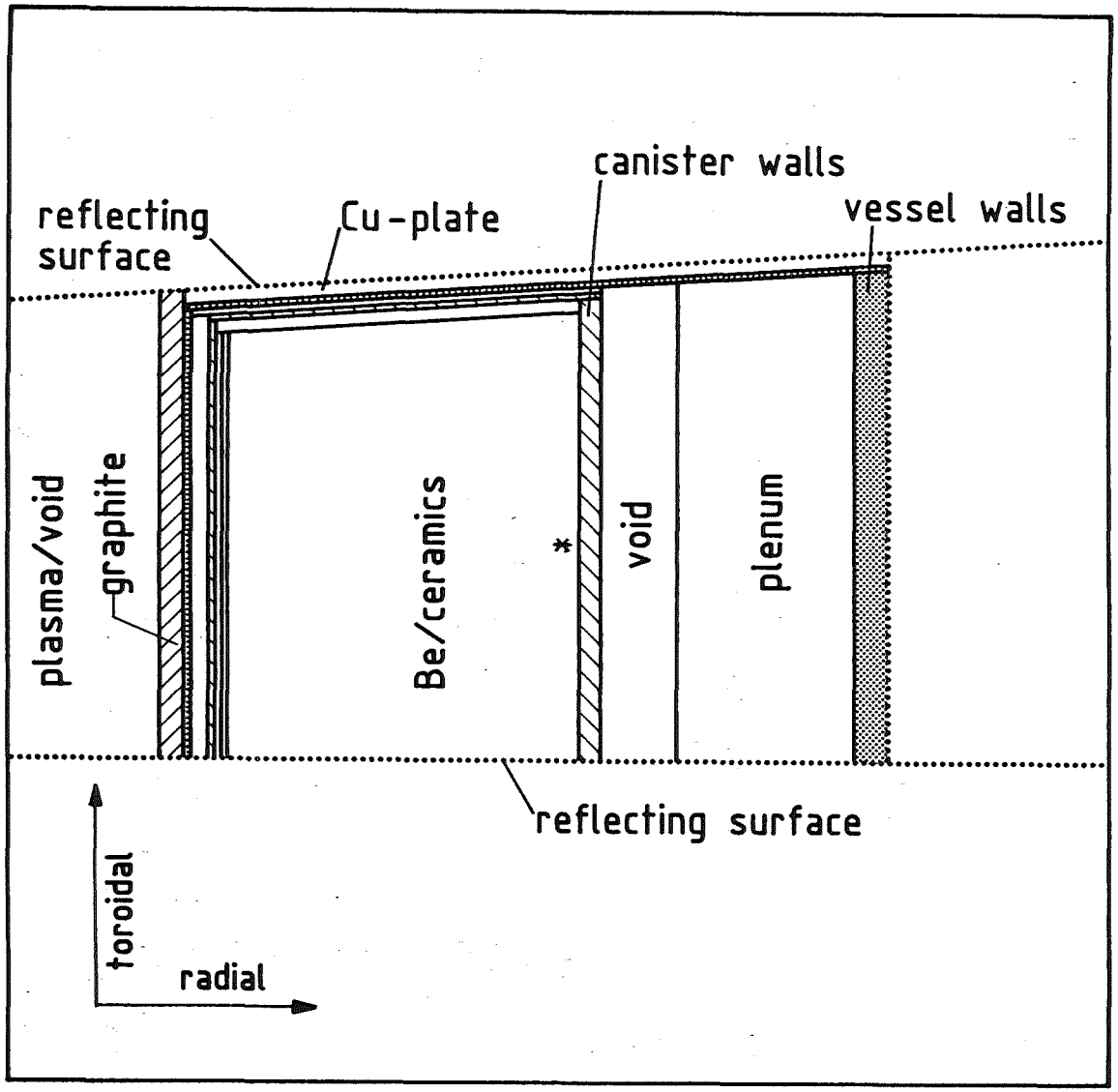

Fig. 6b: Radial-toroidal cross-section of the outboard blanket (half of a 7.5° - sector)

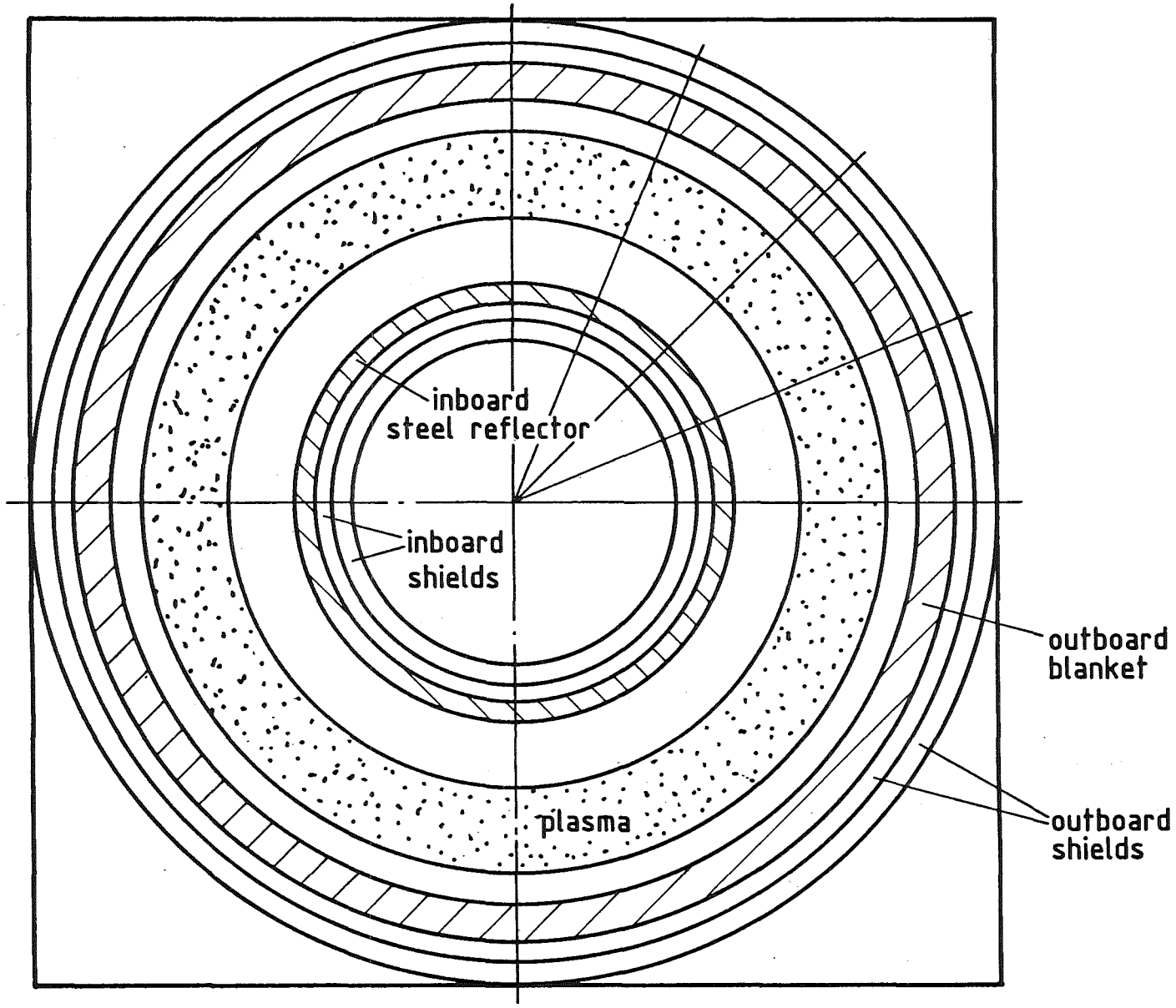

Fig. 7: Radial-toroidal cross-section of the torus in the mid-plane.

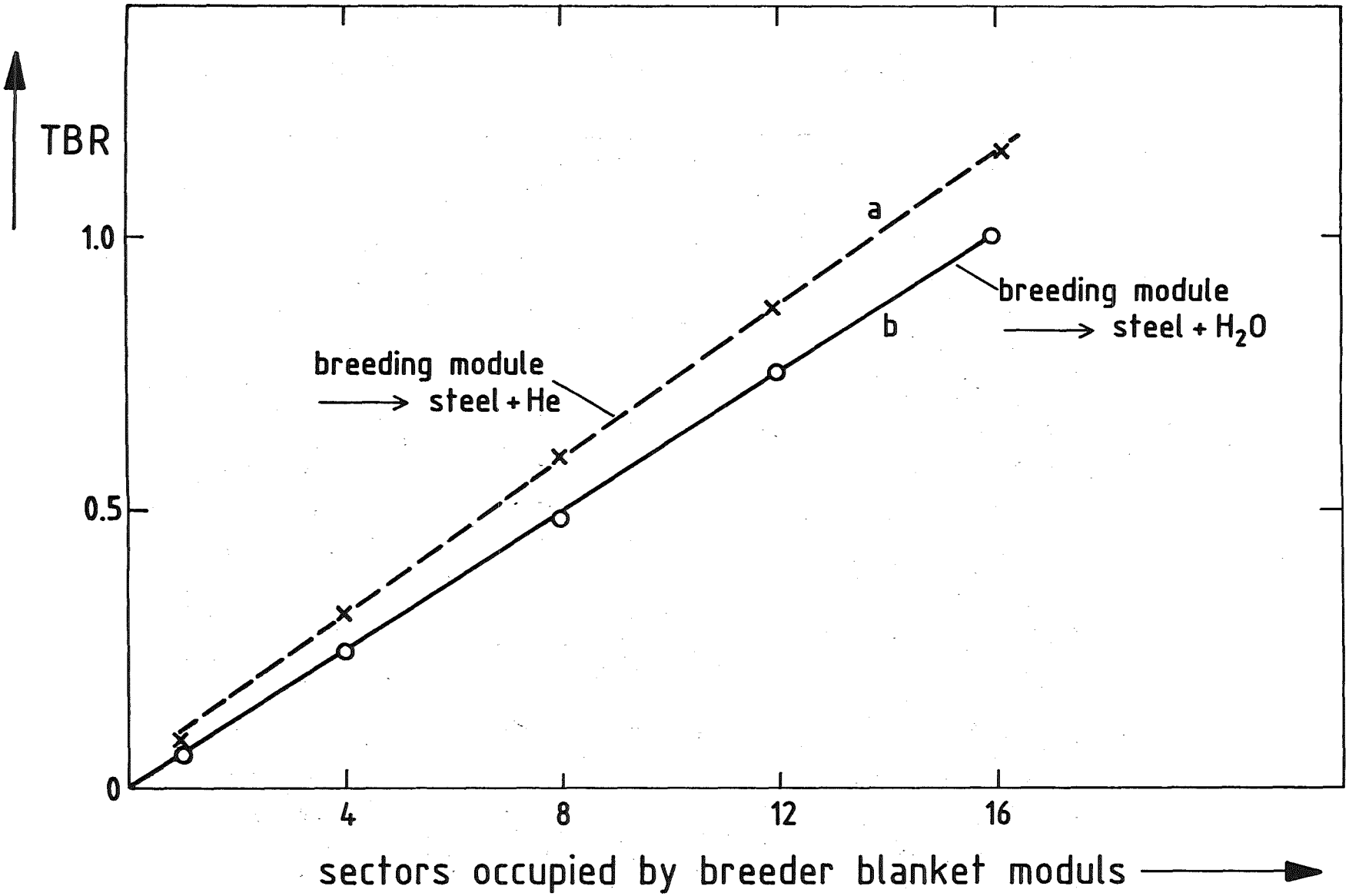

Fig. 8: Tritium Breeding Ratio versus number of outboard sectors occupied by breeding blankets. Rest of outboard sectors and inboard:
a) helium cooled stainless steel shield
b) water cooled stainless steel shield

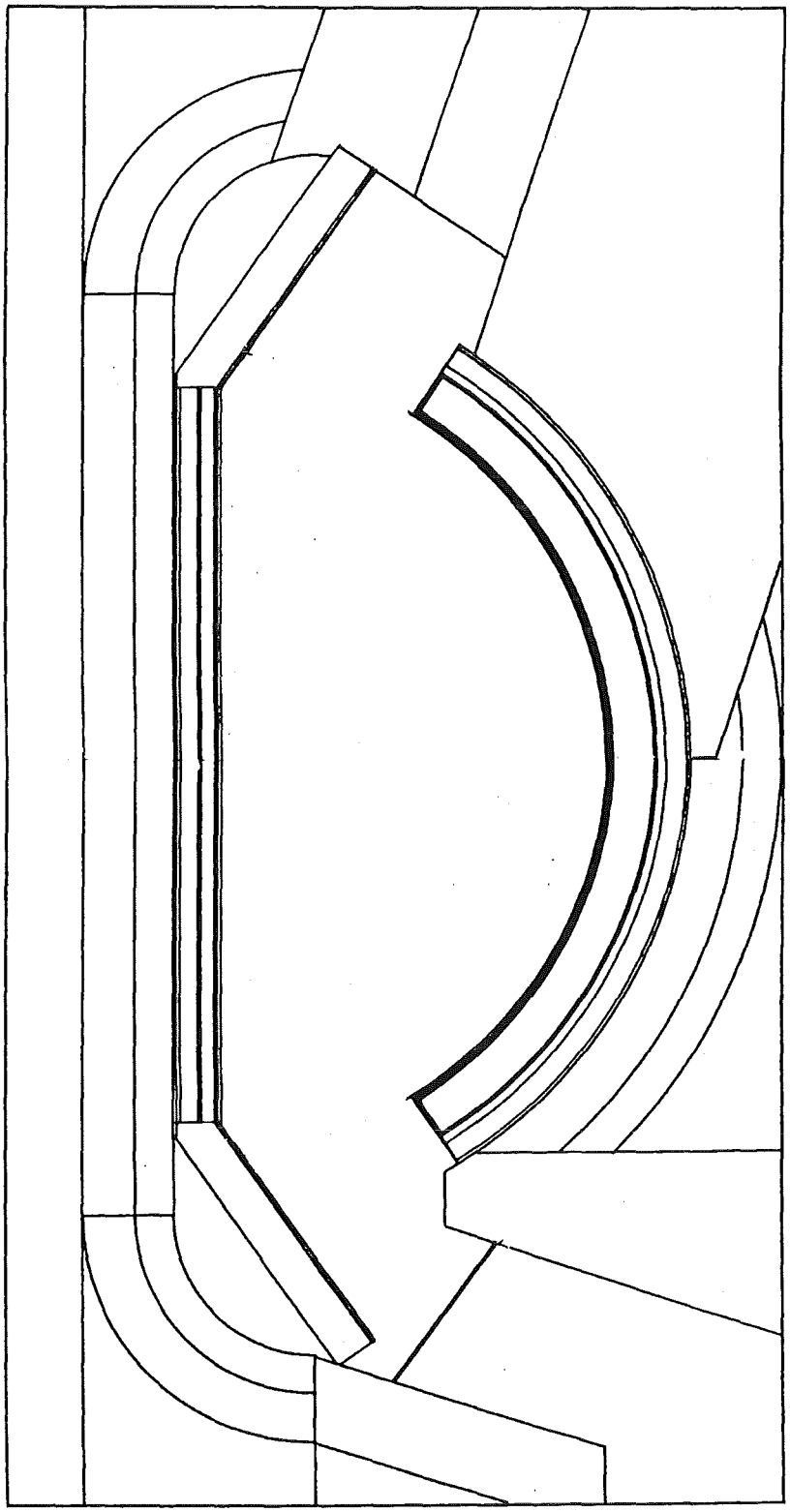

FIG. 9: POLOIDAL-RADIAL CROSS-SECTION OF A SECTOR USED IN THE MONTE-CARLO CALCULATIONS (NET-III/DN CONFIGURATION).

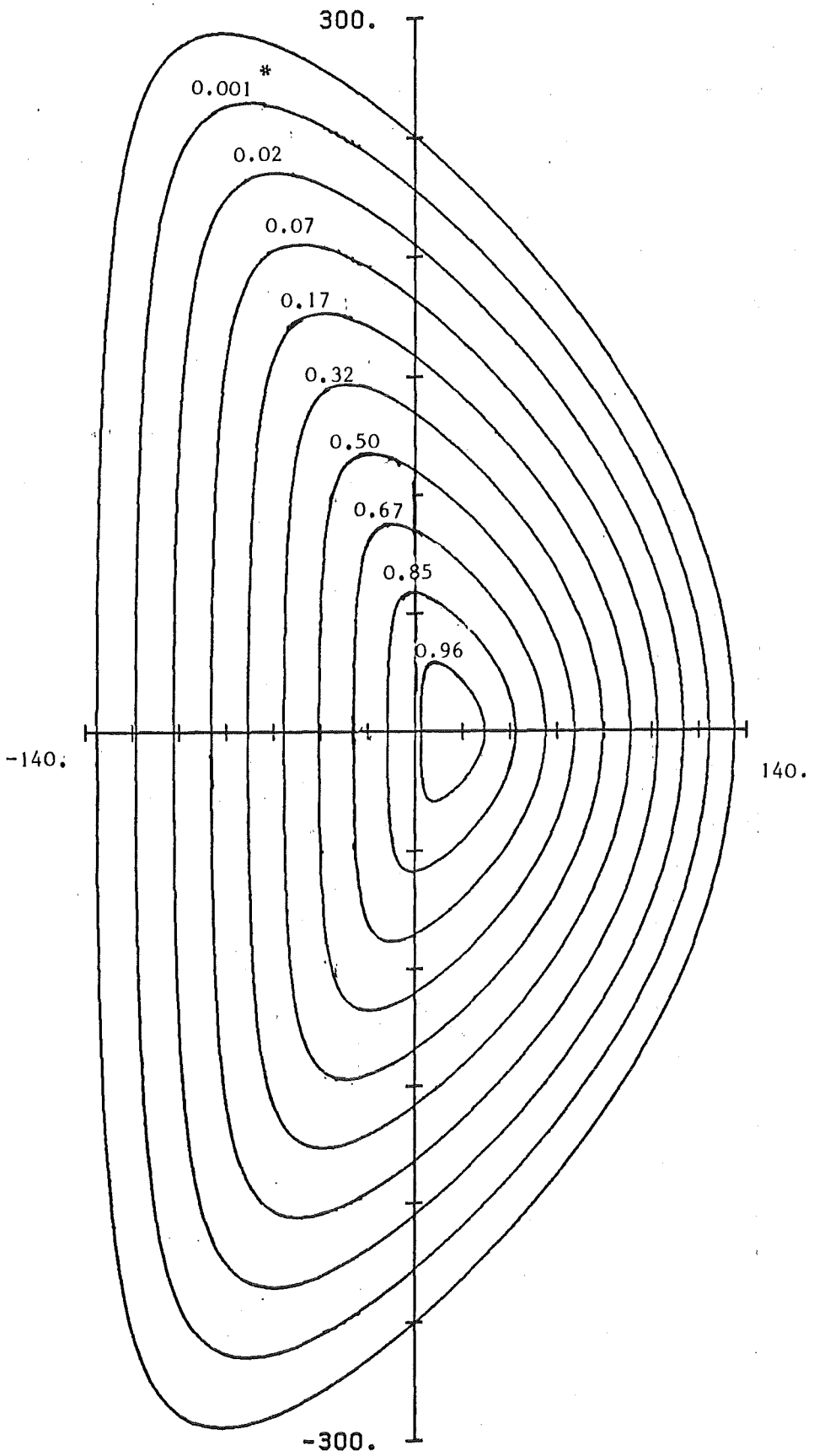

FIG. 10: PLASMA CONTOUR LINES (NET-III/DN).

*The figures at the contour lines designate the normalized source density.

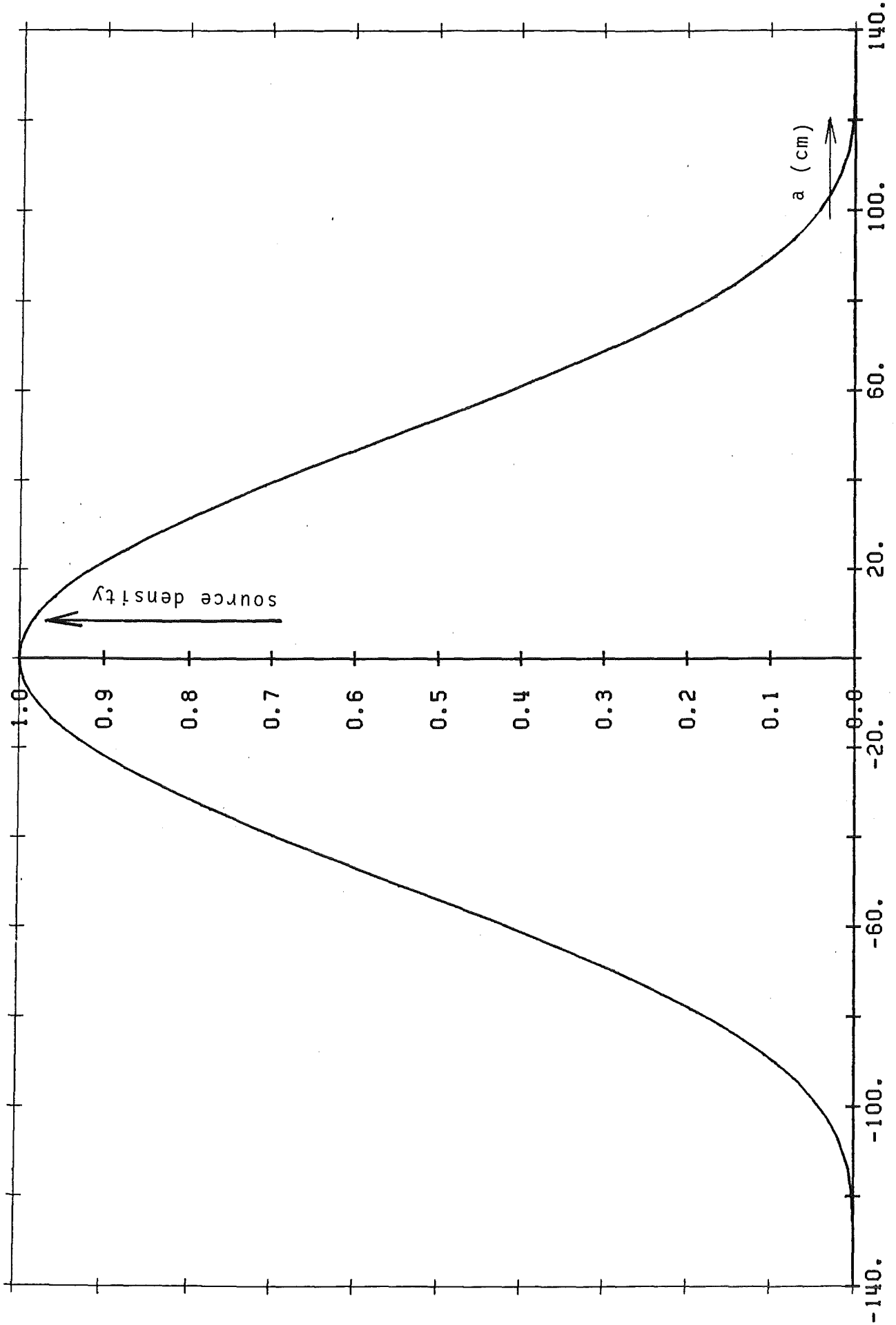

FIG. 11: PLASMA SOURCE DENSITY PROFILE.

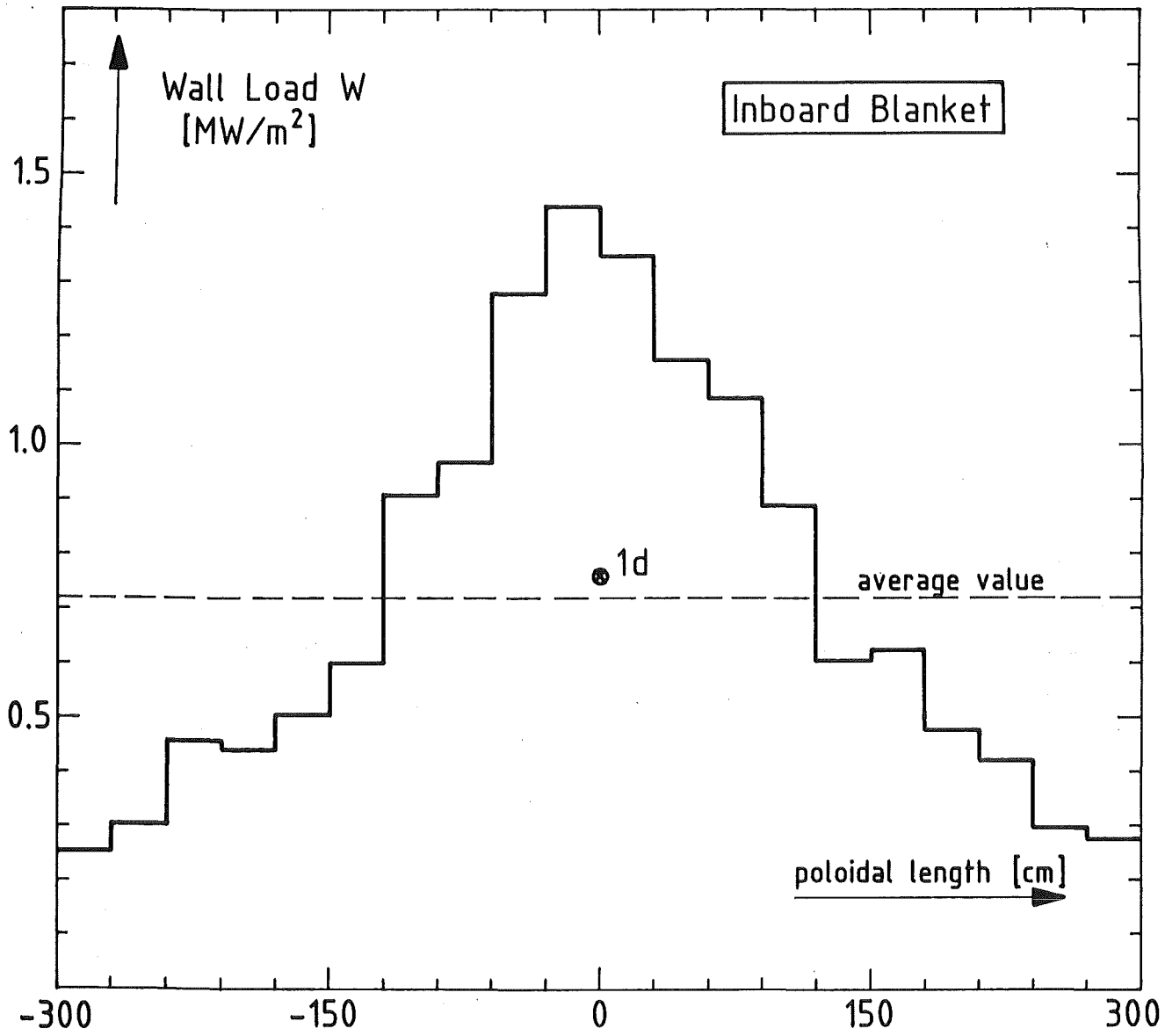

Fig. 12a: Poloidal distribution of the neutron wall load at the inboard first wall (NET-III /DN -configuration).

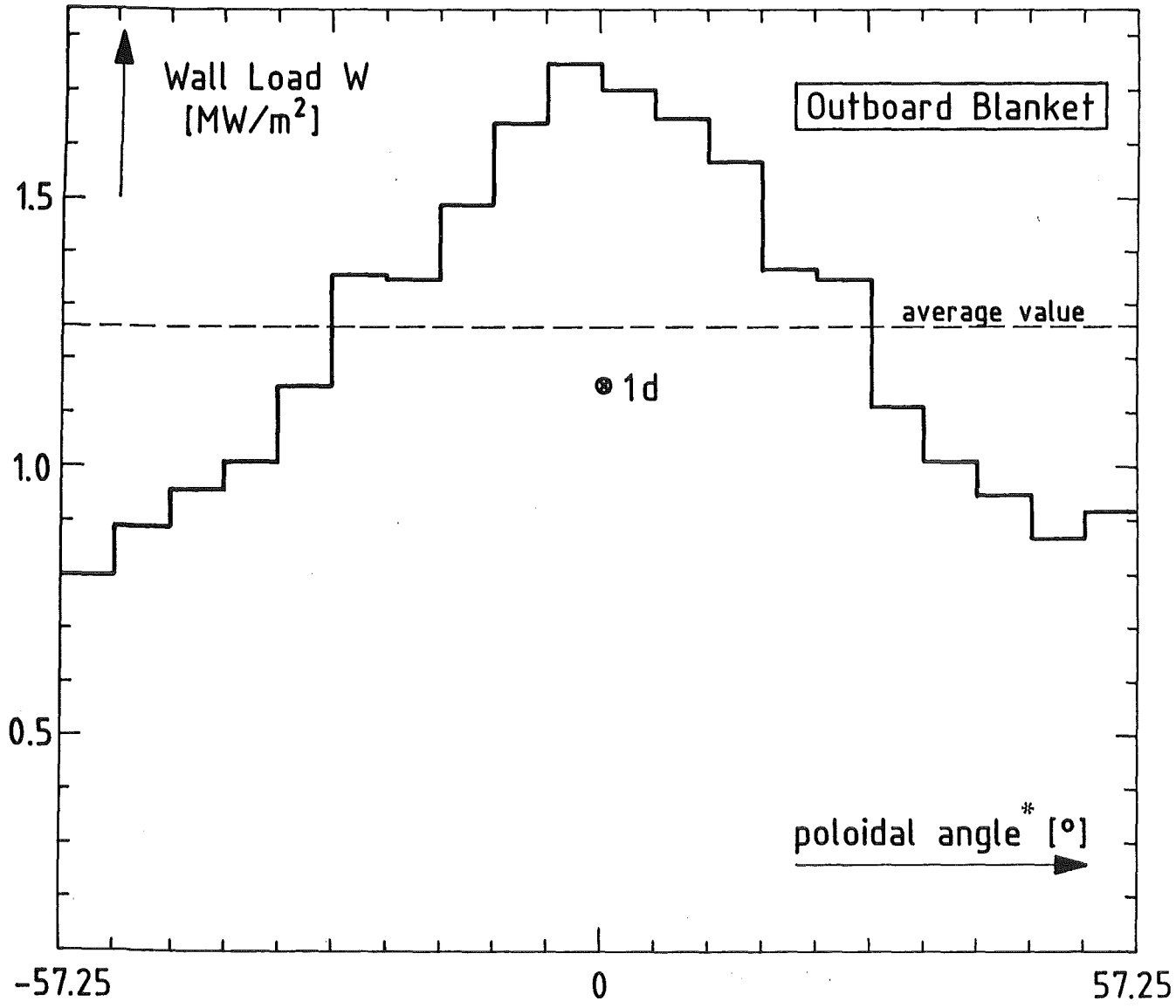

Fig. 12b: Poloidal distribution of the neutron wall load at the outboard first wall (NET-III/DN-configuration).

*A poloidal angle of 5.725° corresponds to a length of 32.57 cm at the outboard first wall.

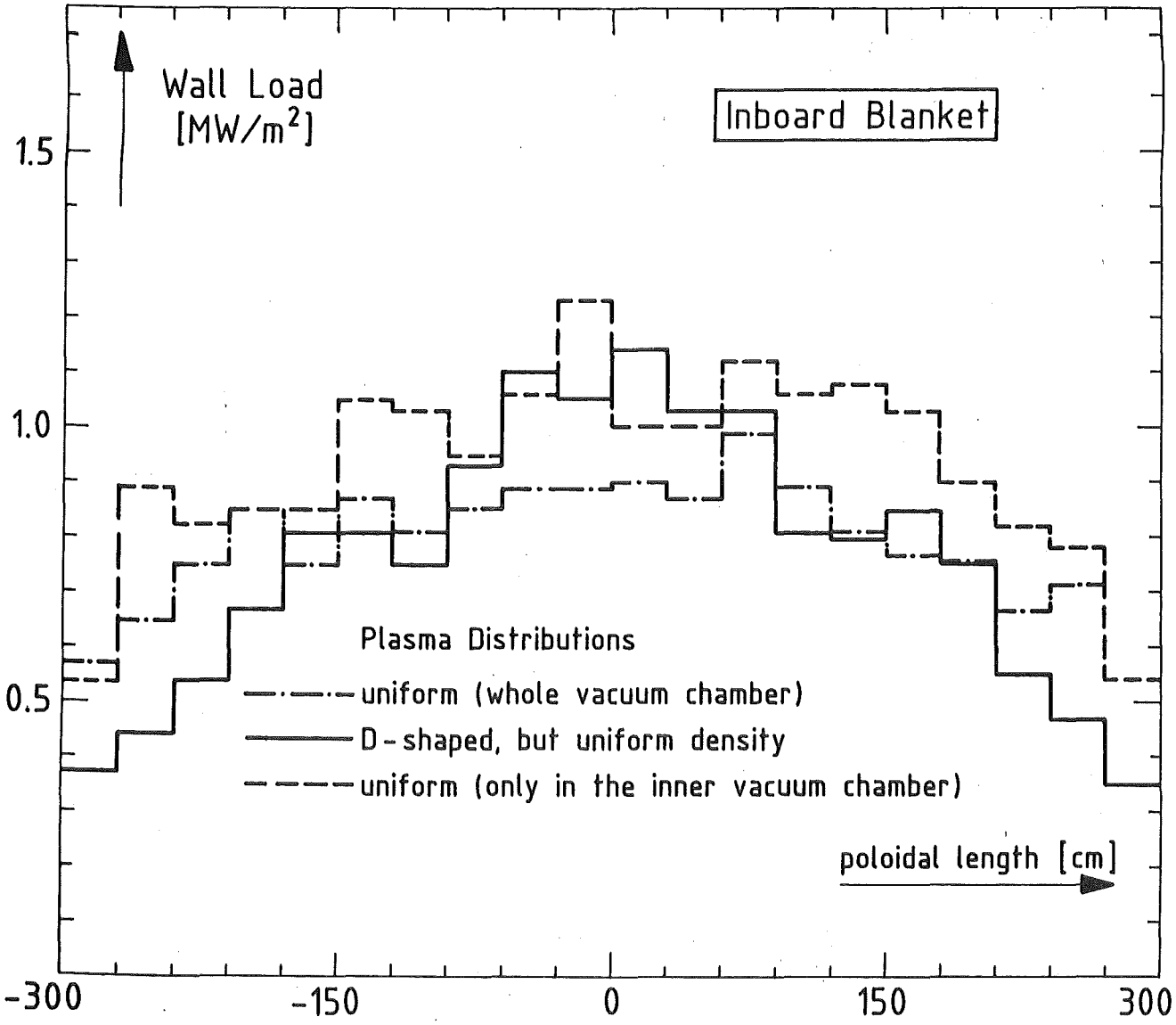

Fig. 13a: Poloidal distribution of the neutron wall load at the inboard first wall for different "artificial" plasma distributions.

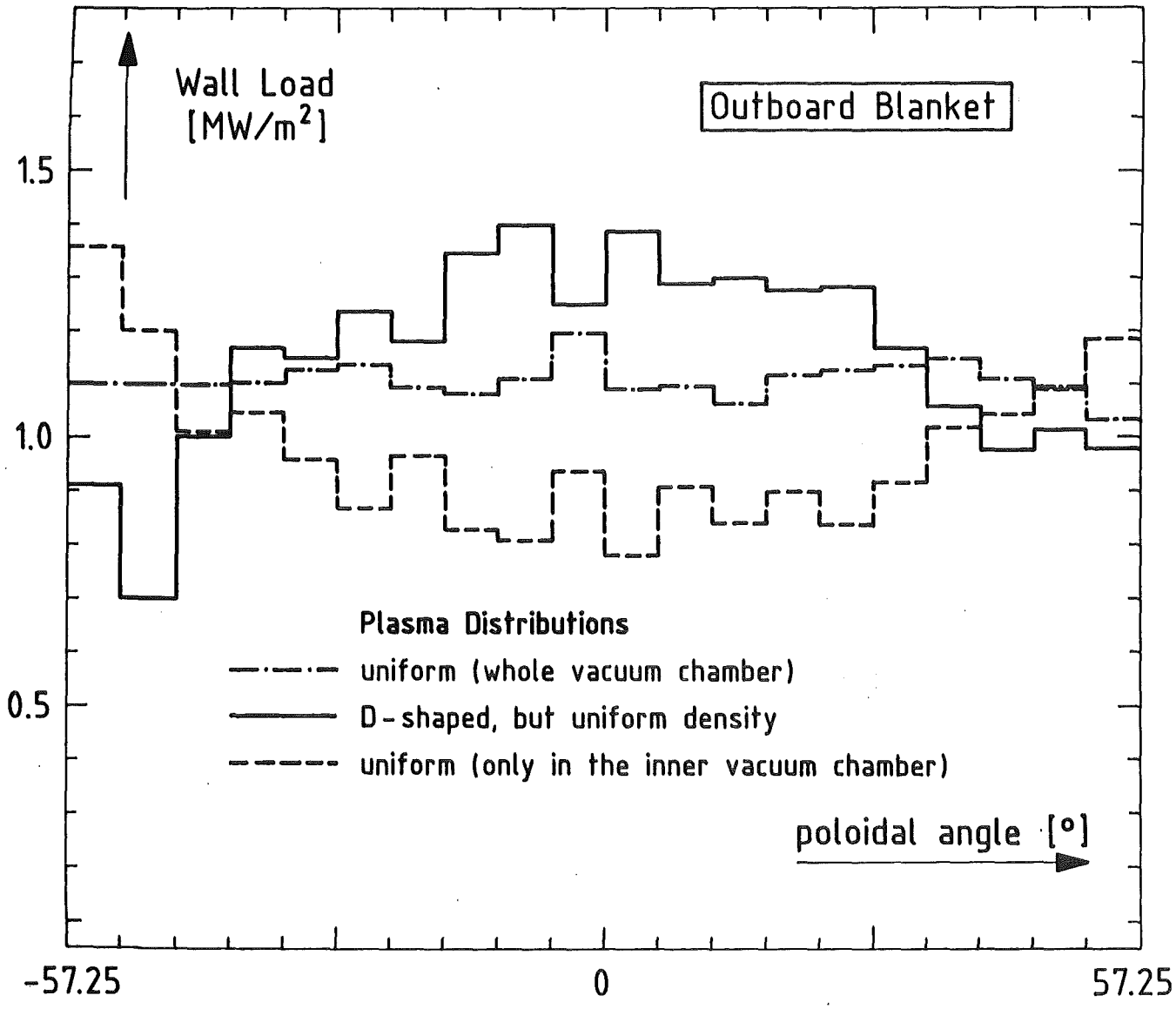

Fig. 13b: Poloidal distribution of the neutron wall load at the outboard first wall for different "artificial" plasma distributions.

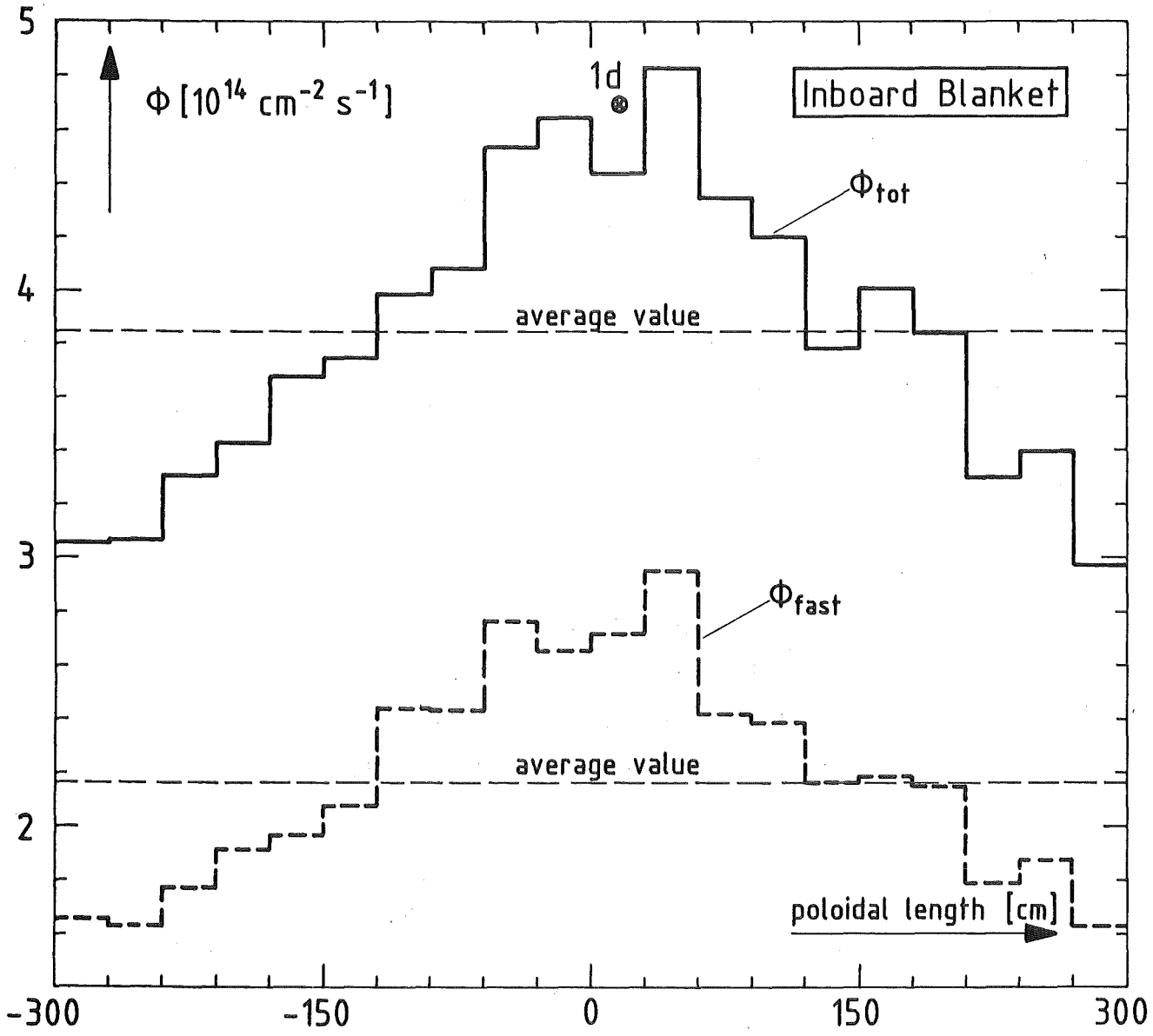

Fig. 14a: Poloidal distribution of the total and fast (E > 0.1 MeV) neutron fluxes at the inboard first wall (NET-III / DN -configuration).

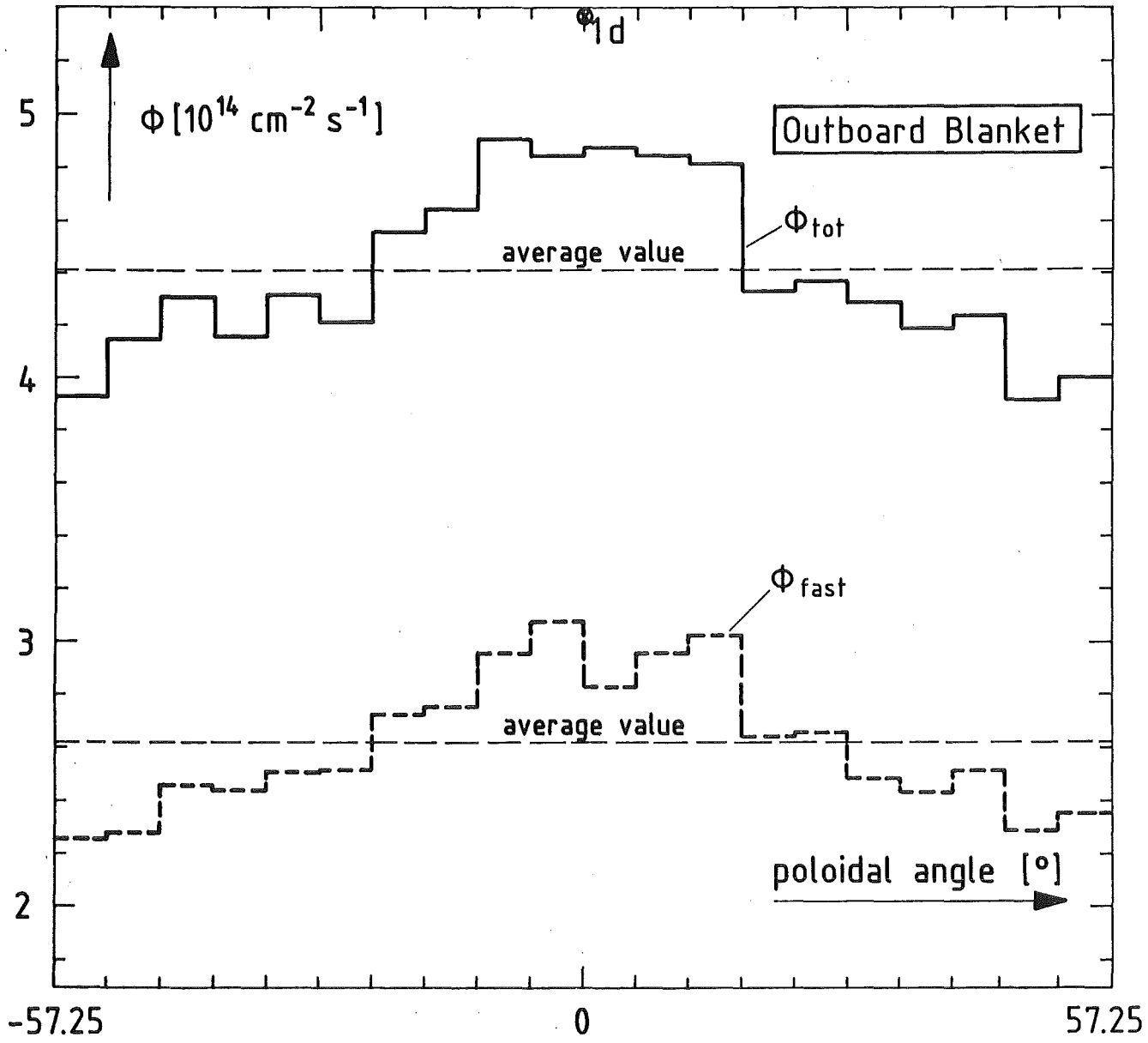

Fig. 14b: Poloidal distribution of the total and fast (E > 0.1 MeV) neutron fluxes at the outboard first wall (NET-III/DN -configuration).

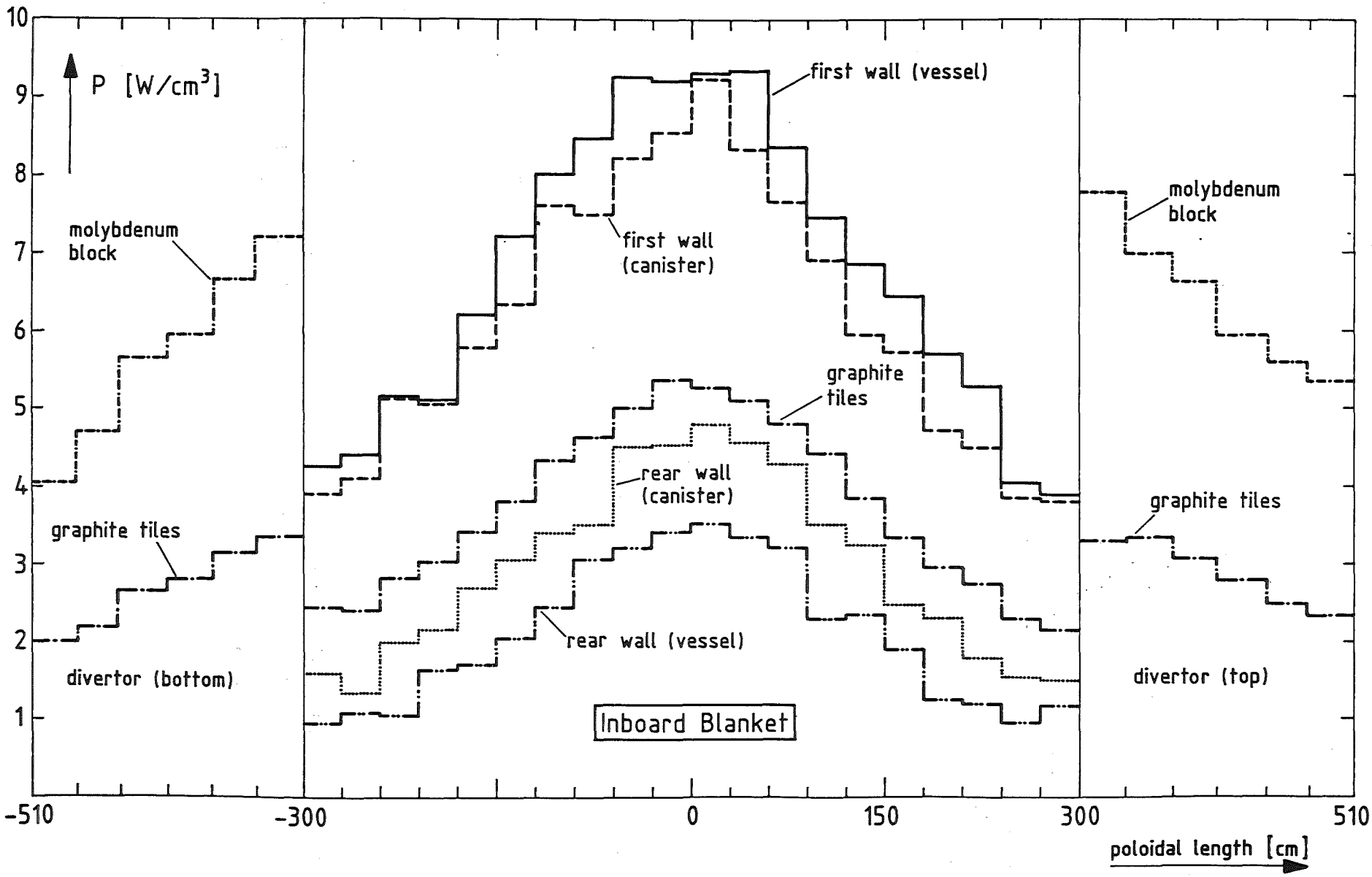

Fig. 15a: Poloidal distribution of the power density in the inboard blanket and the divertors.

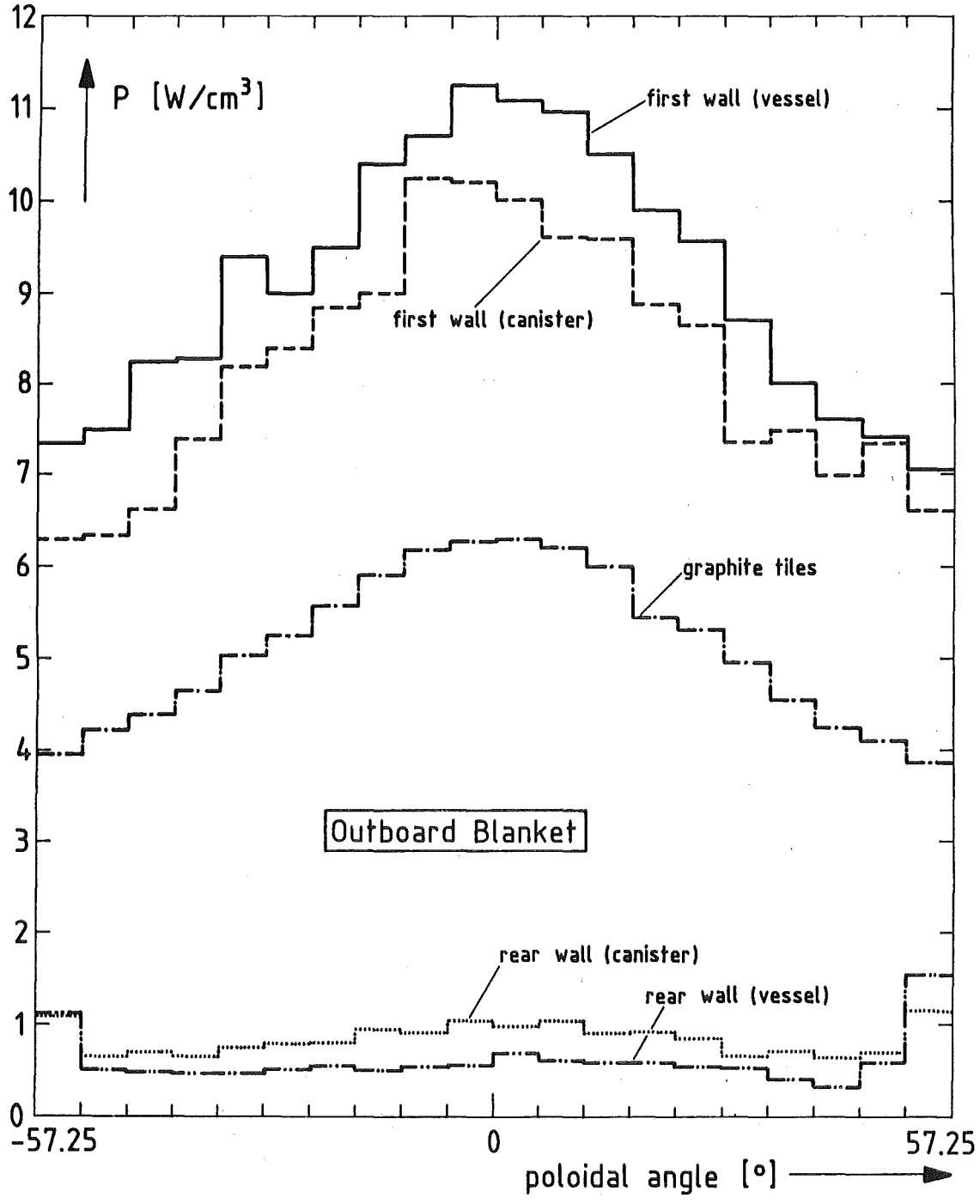

Fig. 15b: Poloidal distribution of the power density in the outboard blanket.

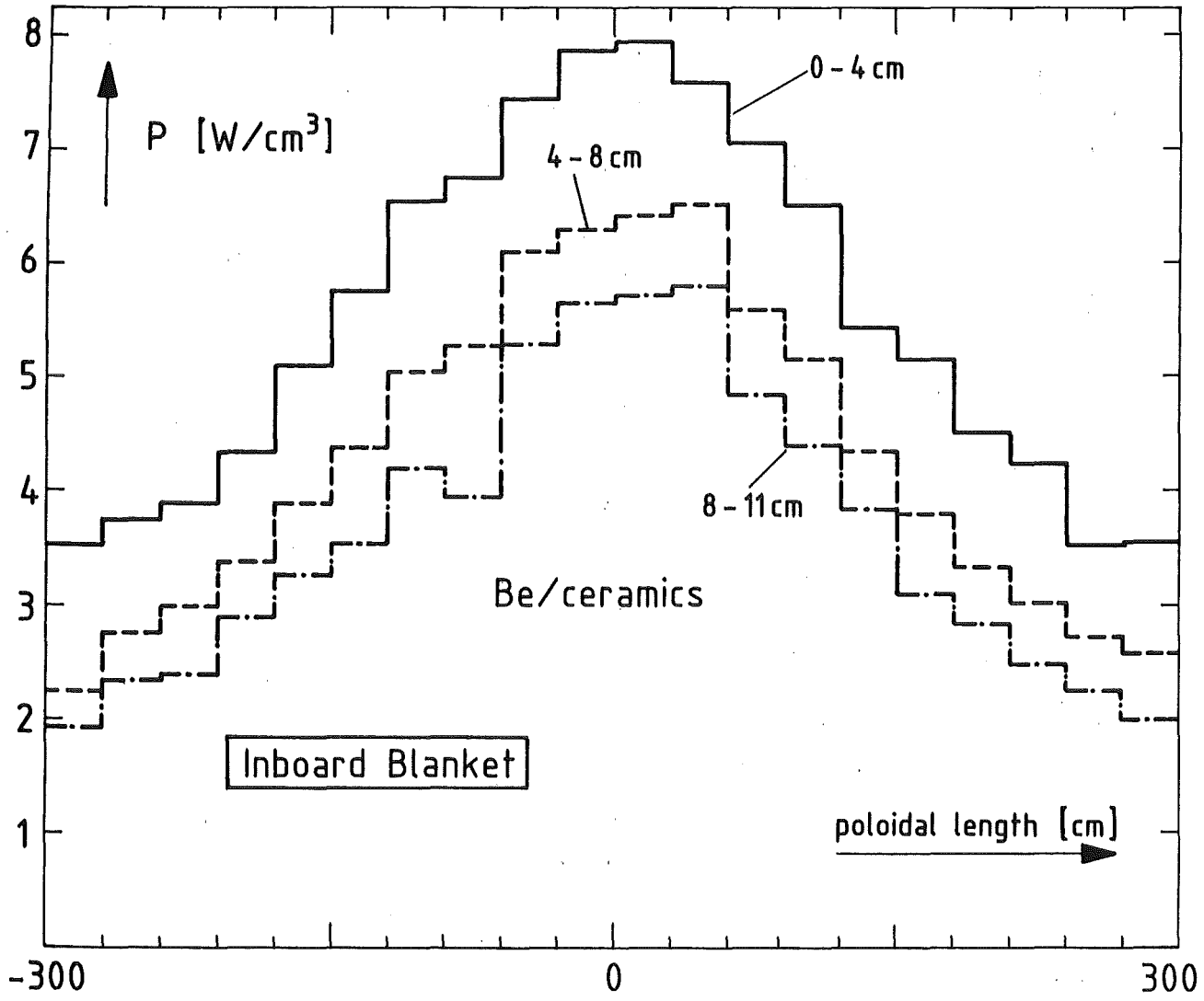

Fig. 16a: Poloidal distribution of the power density in the Be/ceramics - zone at different radial divisions.

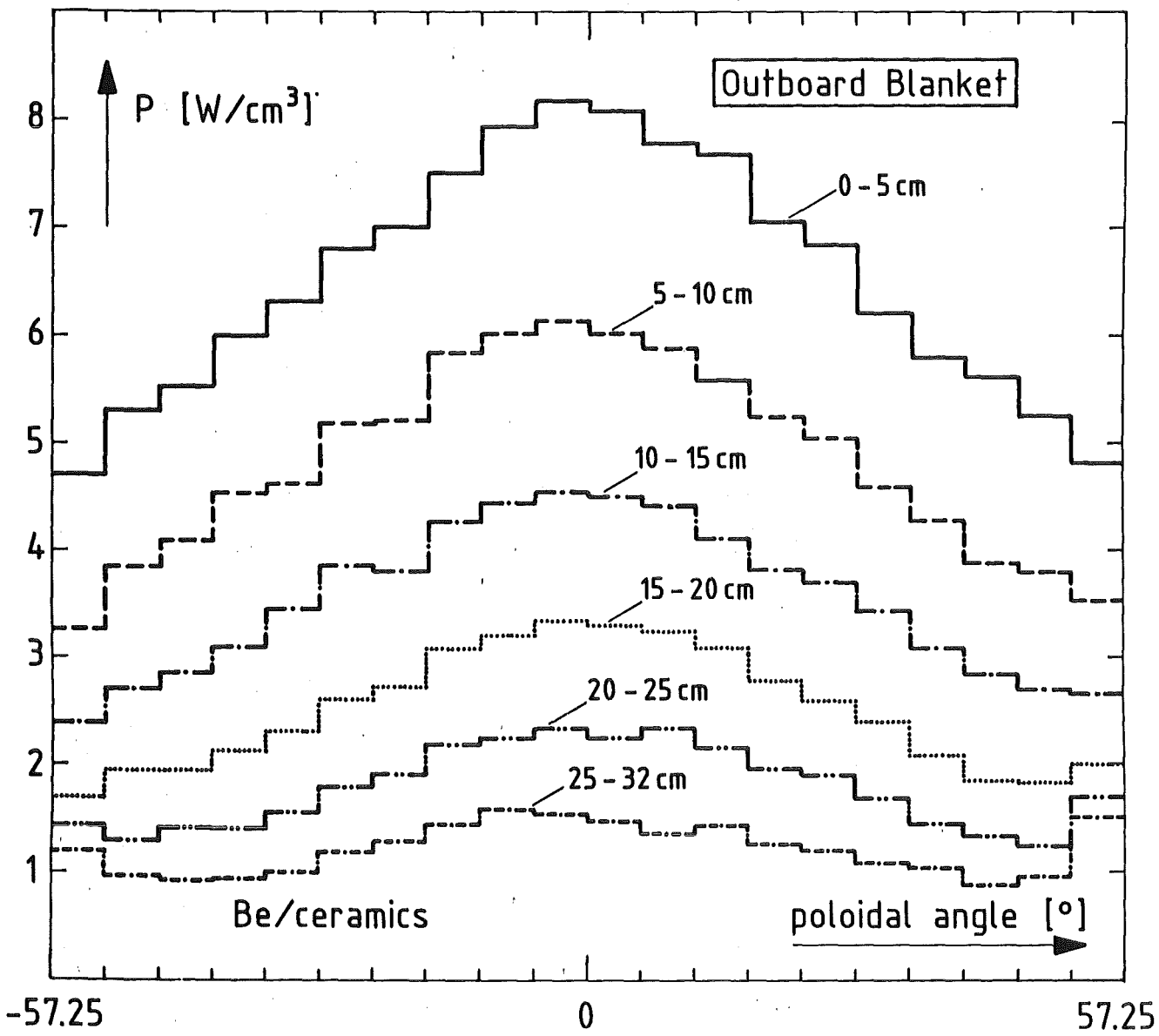

Fig. 16b: Poloidal distribution of the power density in the Be/ceramics-zone at different radial divisions.

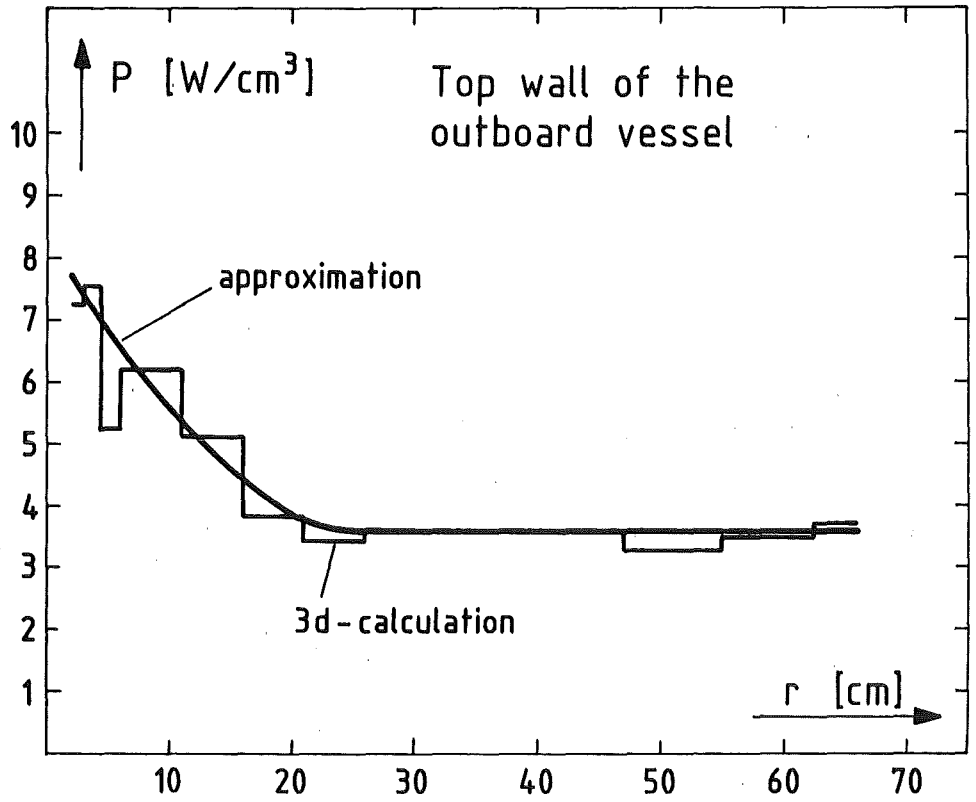

Fig. 17a: Radial distribution of the power density in the wall of the vessel

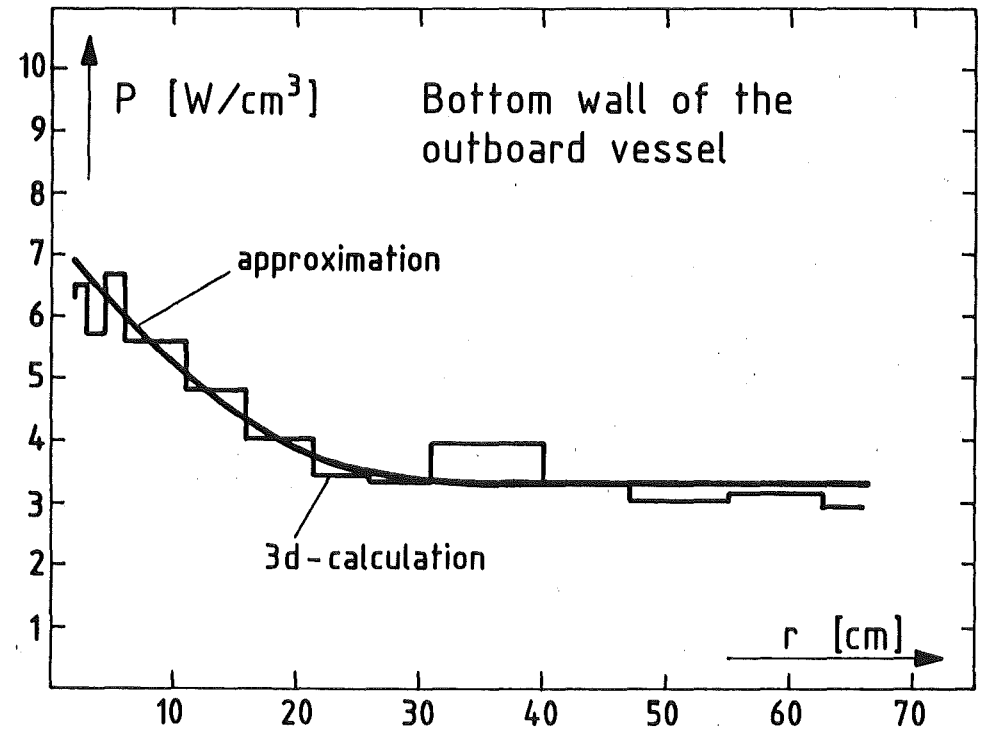

Fig. 17b: Radial distribution of the power density in the bottom wall of the vessel

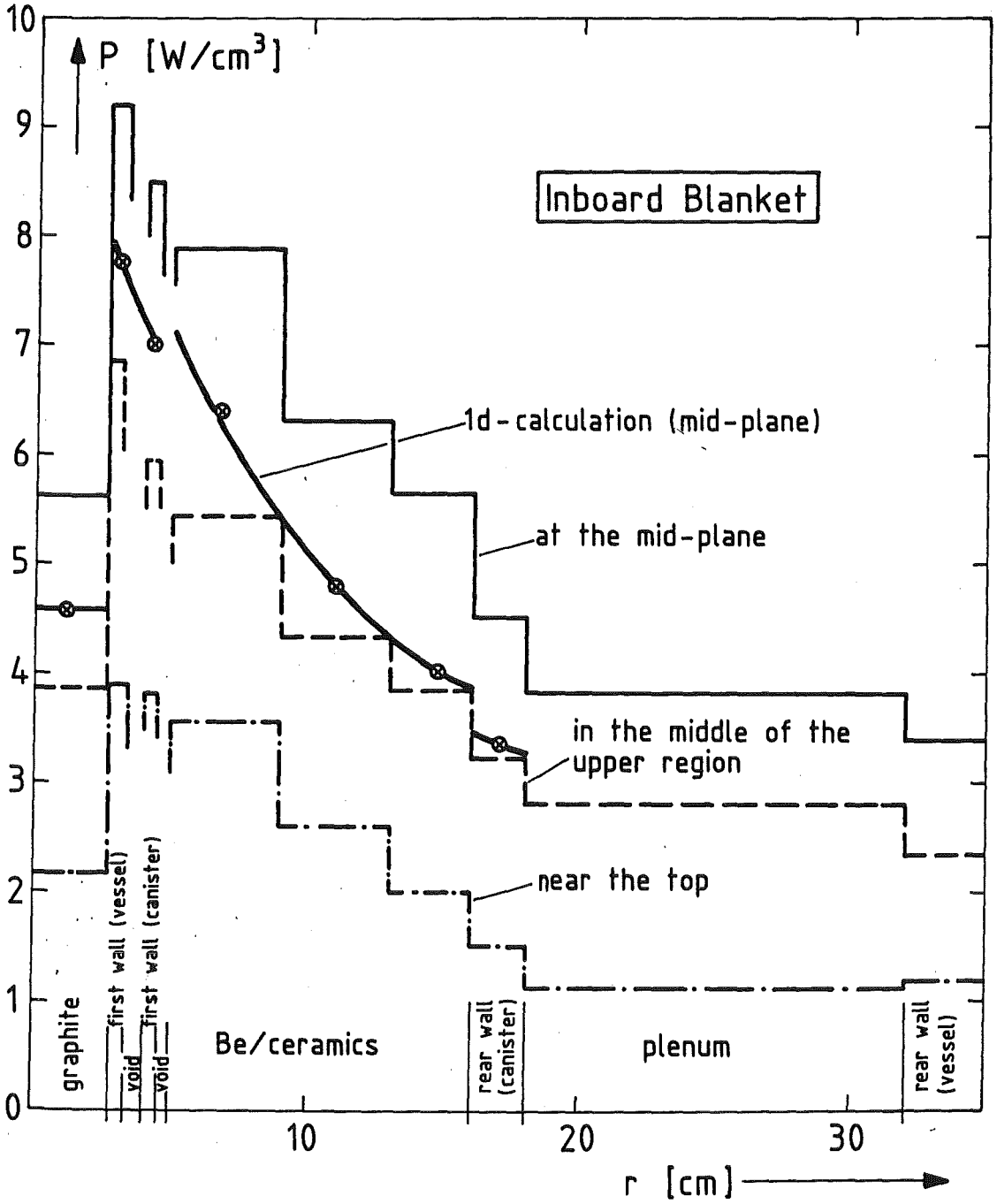

Fig. 18a: Radial profile of the power density in the inboard blanket for different poloidal positions.

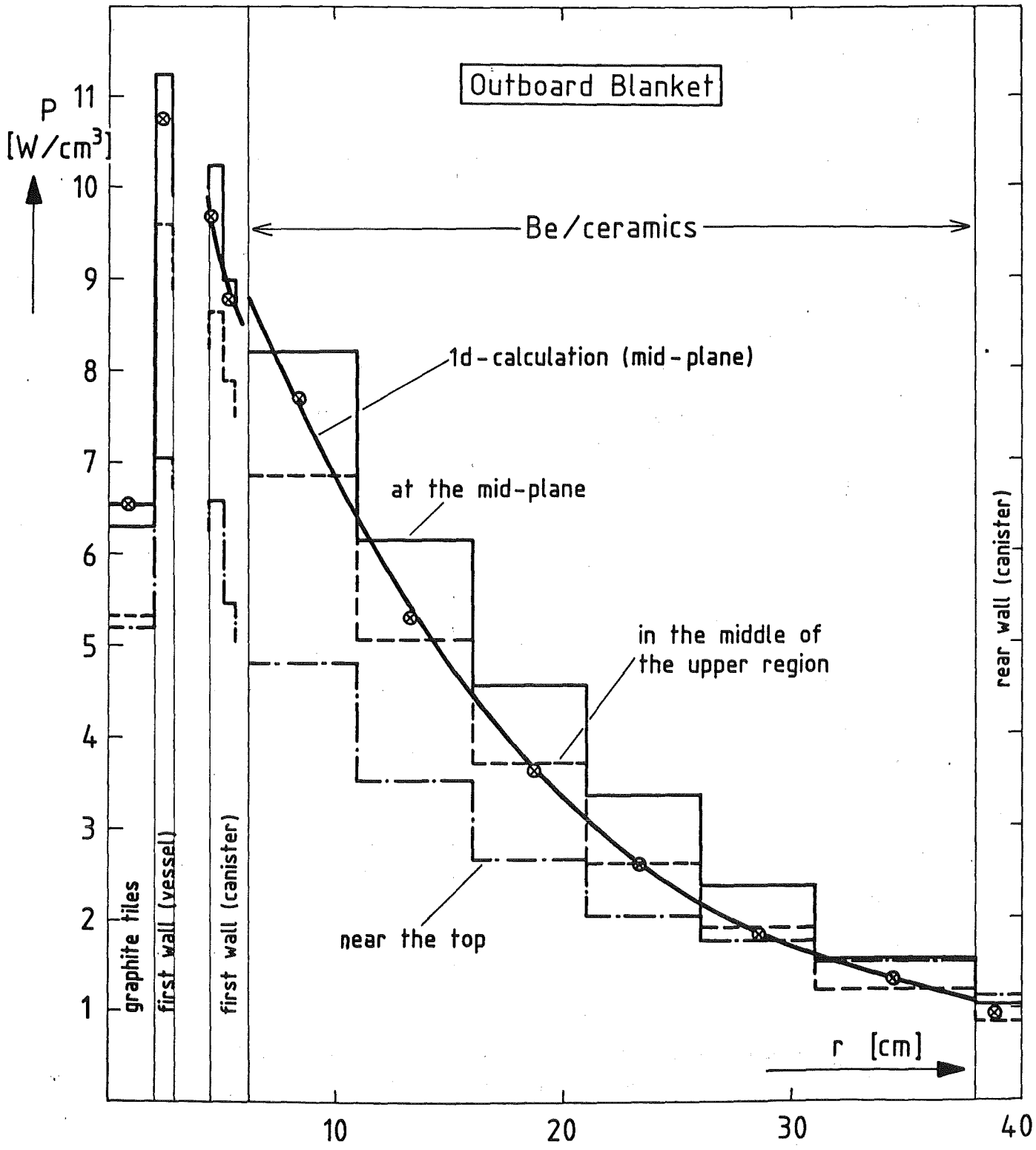

Fig. 18b: Radial profile of the power density in the outboard blanket for different poloidal positions.

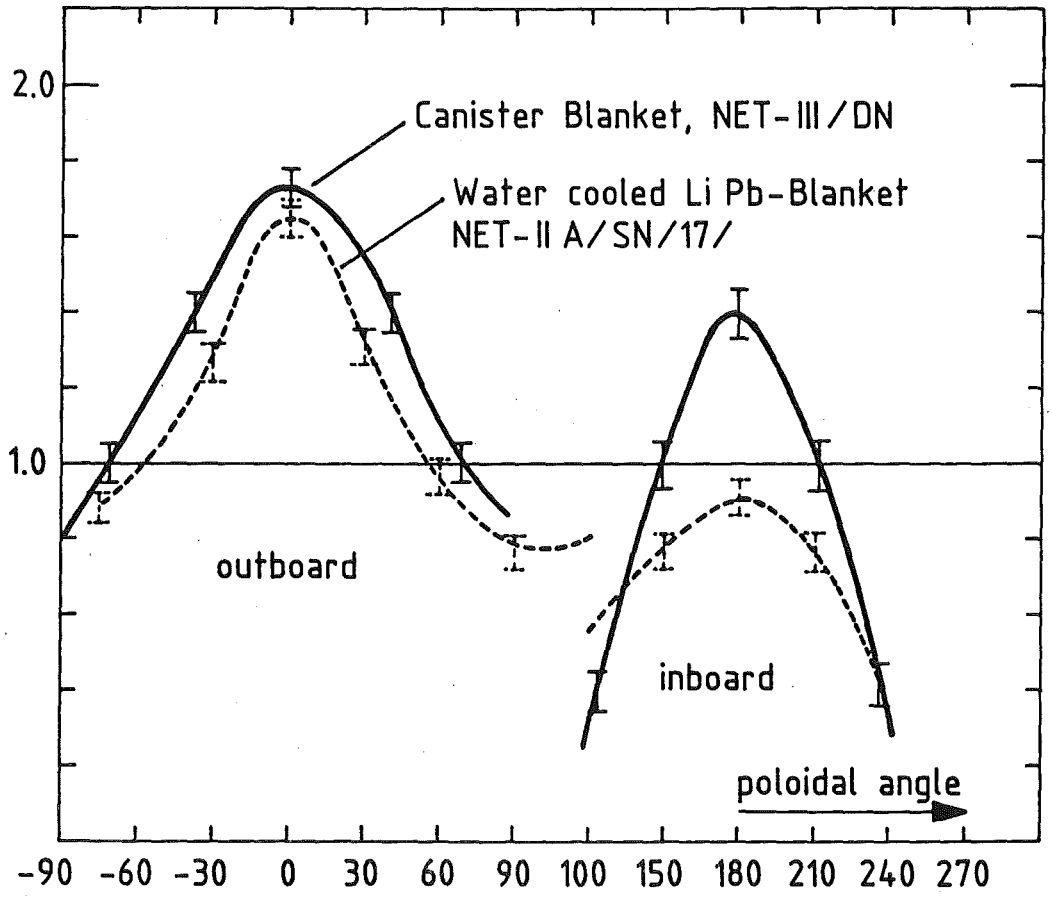

Fig. 19: Comparison of the neutron wall load for the "Canister Blanket" in the NET-III/DN configuration and a previous calculation by C. Ponti for a water-cooled LiPb-blanket in a single null configuration (NET-II A). The average neutron wall load is normalized to 1.0 MW/m^2 in both cases.